Research article

JGS
Journal of the Geological Society

https://doi.org/10.1144/jgs2022-023 | Vol. 180 | 2023 | jgs2022-023

Geochemical and radiogenic isotope records of the Weissert Event in south Tethyan sediments

M. Shmeit[1,2*], C. Chauvel[1,3], F. Giraud[1], E. Jaillard[1], S. Reboulet[4], M. Masrour[5], J. E. Spangenberg[6] and A. El-Samrani[2]

[1] Université Grenoble Alpes, Université Savoie Mont Blanc, CNRS, IRD, Université Gustave Eiffel, ISTerre, 38000 Grenoble, France
[2] Doctoral School of Science and Technology, Laboratory of Geosciences, Georesources and Environment L2GE, EDST/PRASE, Lebanese University, Beirut, Lebanon
[3] Université de Paris, Institut de Physique du Globe de Paris, CNRS, F-75005 Paris, France
[4] Université Lyon, UCBL, ENSL, UJM, CNRS, LGL-TPE, F-69622 Villeurbanne, France
[5] Faculté des Sciences, Département de Géologie, Université Ibn Zohr, BP 8106, Cité Dakhla, Agadir, Morocco
[6] Institute of Earth Surface Dynamics (IDYST), University of Lausanne, CH-1015 Lausanne, Switzerland

MS, 0000-0003-0291-4968; CC, 0000-0002-3959-4665; FG, 0000-0002-4732-4737; SR, 0000-0002-7232-8596; MM, 0000-0001-6821-9023; JES, 0000-0001-8636-6414; AE-S, 0000-0002-2654-4212

* Correspondence: majd.homaidan-shmeit@u-bourgogne.fr

Abstract: The Cretaceous marine sedimentary record is characterized by time intervals rich in organic matter correlating with positive carbon isotope excursions, often called oceanic anoxic events. The Weissert Event corresponds to the first such event in the Cretaceous during the Valanginian stage. The associated palaeoenvironmental perturbations, which include increasing marine surface water primary productivity, are hypothesized to have been triggered by volcanic activity from large igneous provinces, and the source of nutrients is not well constrained (continental runoff v. oceanic upwelling). We present isotope ratios of Pb, Sr and Nd, together with concentrations of major and trace elements, for sediments from the central Moroccan margin to test these hypotheses. We demonstrate that the nutrient input was dominated by continental weathering. The source of sedimentary material remained stable during the Valanginian interval and originated from an old source, probably the African Sahara region. The radiogenic isotope signatures do not show a significant contribution of volcanic products from any known Valanginian large igneous province to the geochemical budget of sediments deposited on the central Moroccan margin. Although this does not preclude an impact of volcanic activity on the composition of seawater, it demonstrates that the erupted volumes were not sufficient to affect the deposited sediments.

Supplementary material: The Supplementary Table contains three sheets: (1) Central Moroccan Margin, the analytical data generated and analysed during this study; (2) Fig. 8 data, large igneous provinces, the data of known Valanginian large igneous provinces used for comparison; and (3) Fig. 9 and S5 data, source areas, the data of potential surrounding source areas used for comparison, available at https://doi.org/10.6084/m9.figshare.c.6333040.

Received 14 February 2022; **revised** 10 October 2022; **accepted** 29 November 2022

The Cretaceous marine sedimentary record is characterized by several positive carbon isotope excursions (CIEs) corresponding to perturbations in the global carbon cycle (Scholle and Arthur 1980; Weissert *et al.* 1998). These are mainly explained by enhanced marine and terrestrial primary productivity and/or the enhanced preservation of organic matter (Scholle and Arthur 1980; Weissert 1989; Kump and Arthur 1999). Positive CIEs are often associated with records of widespread organic-rich oceanic sediments referred to as oceanic anoxic events (OAEs; Schlanger and Jenkyns 1976; Scholle and Arthur 1980). The Valanginian stage (137.7–132.6 Ma; Gale *et al.* 2020) records the first positive CIE of the Cretaceous and is named the Weissert OAE (Lini *et al.* 1992; Weissert *et al.* 1998; Erba *et al.* 2004). However, its expression as an OAE is doubted due to the absence of significant and widespread organic-rich layers (Westermann *et al.* 2010; Kujau *et al.* 2012). The most significant organic-rich layers in the Tethys Realm are the centimetre-scale Barrande layers (1.9–3.7% total organic carbon) observed prior to the Valanginian positive CIE in the Vocontian basin (SE France) (Reboulet *et al.* 2003).

The positive CIE corresponding to the Weissert Event is observed in a wide range of geographical locations, such as the Tethys, Atlantic, Pacific and Boreal realms and the southern hemisphere (Hennig *et al.* 1999; Bartolini 2003; Price and Mutterlose 2004; Sprovieri *et al.* 2006; McArthur *et al.* 2007; Aguirre-Urreta *et al.* 2008; Bornemann and Mutterlose 2008; Charbonnier *et al.* 2013; Price *et al.* 2018). Following Martinez *et al.* (2015), the onset of the Valanginian CIE is recorded at 135.22 ± 1.0 Ma and is characterized by three phases: (1) a rapid increase in $\delta^{13}C_{carb}$ lasting 0.60 myr; (2) stable $\delta^{13}C_{carb}$ values with a duration of 1.48 myr; and (3) a smooth decrease in $\delta^{13}C_{carb}$ lasting 3.77 myr. This CIE is recorded in marine carbonates and organic matter (Lini *et al.* 1992; Channell *et al.* 1993; Gréselle *et al.* 2011; Aguado *et al.* 2018) and in terrestrial fossil plants (Gröcke *et al.* 2005), implying a perturbation in both the oceanic and atmospheric carbon reservoirs.

The Weissert Event is associated with a warm and humid climate (Lini *et al.* 1992; Charbonnier *et al.* 2020), enhanced marine primary productivity (Bersezio *et al.* 2002; Bartolini 2003; Erba and Tremolada 2004; Duchamp-Alphonse *et al.* 2007; Bornemann and Mutterlose 2008; Mattioli *et al.* 2014) and a biocalcification crisis in platform and pelagic settings (Channell *et al.* 1993; Weissert *et al.* 1998; Wortmann and Weissert 2000; Erba and Tremolada 2004; Föllmi *et al.* 2006). Two main hypotheses explain the eutrophication (i.e. nutrient input) of the marine environment in proximal and distal marine settings. Intensification of the hydrological cycle is suggested to cause higher detrital and nutrient input in proximal settings close to fluvial influxes (Lini *et al.* 1992; Jenkyns 2003;

Erba *et al.* 2004). By contrast, nutrient input in pelagic settings is often explained by the introduction of nutrients from oceanic upwelling (Arthur *et al.* 1990; Weissert *et al.* 1998; Jenkyns 2010; Föllmi 2012). Such proposed hypotheses for the fertilization of the ocean need to be examined for the Weissert Event.

The triggering conditions causing the environmental perturbations of the Weissert Event are tentatively linked with extensive volcanism from the Paraná–Etendeka large igneous province (LIP; Weissert *et al.* 1998; Erba *et al.* 2004; Charbonnier *et al.* 2017) or the Comei–Bunbury LIP (Zhu *et al.* 2009). The radiometric ages of basalts from these LIPs cluster around 135.5–126 Ma (Liu *et al.* 2015; Almeida *et al.* 2018; Baksi 2018; Rocha *et al.* 2020; Bacha *et al.* 2022), probably post-dating the onset of the Valanginian positive CIE (135.22 ± 1.0 Ma; Martinez *et al.* 2015). Previous studies used Pb isotopes from the Ocean Drilling Program Leg 185 Hole 1149B (western Pacific) to demonstrate a link between the Weissert Event and the Paraná–Etendeka LIP (Chavagnac *et al.* 2008; Peate 2009). However, constraints provided by Sr and Nd isotopes are not necessarily consistent with such an interpretation and the number of Valanginian samples showing a Pb isotopic shift is very low.

We report here the major and trace element concentrations and radiogenic isotope ratios of Pb, Sr and Nd in Valanginian carbonate sediments from two stratigraphic successions on the central Moroccan margin. Comparing data obtained for sediments from an onshore section (Zalidou; the Essaouira–Agadir Basin) and an offshore Deep Sea Drilling Project succession (DSDP Leg 50 Hole 416A, east Atlantic) allowed an investigation of the geochemical similarities and differences between a proximal and a distal site on the same margin. At both sites, the temporal geochemical variations are constrained by an accurate chronostratigraphic framework, allowing us to establish whether changes occurred before, during or after the Weissert Event. Ultimately, the aim of this study was (1) to determine whether the source of nutrients (i.e. eutrophication) was continental runoff, oceanic upwelling, or both, and (2) to search for a volcanic contribution in the sediments, a feature that would support a volcanic origin for the Weissert Event.

Geological setting

The Essaouira–Agadir Basin faces the eastern Atlantic margin and is located in the western High Atlas of Morocco (30° 30′–31° 05′ N, 9° 55′–9° 20′ W) (Fig. 1). The Essaouira–Agadir Basin extends offshore until the western limit of the continental margin and constitutes part of the present day Atlantic passive margin (Frizon de Lamotte *et al.* 2008). Consequently, the geological evolution of the passive margin controlled that of the basin itself (Ellouz *et al.* 2003). Post-rift sedimentation, along with thermal subsidence, started in the mid-Jurassic and a eustatic transgression gave way to extended marine sedimentation during the Early Cretaceous (Berriasian–early Hauterivian; Piqué *et al.* 1998; Hafid *et al.* 2008; Frizon de Lamotte *et al.* 2009). During the Early Cretaceous, the basin corresponded to a temperate platform on the south Tethyan margin between palaeolatitudes *c.* 15° N and *c.* 22° N (Fig. 2).

Sedimentary rocks of Valanginian age (137.7–132.6 Ma) were sampled from two different geological successions on the central Moroccan margin, one onshore and proximal (the Zalidou section) and the other offshore and distal (DSDP Hole 416A) (Fig. S1). Both geological successions have a well-constrained biostratigraphy (ammonites for the onshore succession, and calcareous nannofossils for both successions) and chemostratigraphy (carbon isotopes), allowing the identification of the Weissert Event (Reboulet *et al.* 2022; Shmeit *et al.* 2022). The combination of these two successions allowed an investigation of how the geochemical signature in a proximal setting close to fluvial discharge compares with that in a distal setting close to possible oceanic upwelling (Price *et al.* 1995; Poulsen *et al.* 1998).

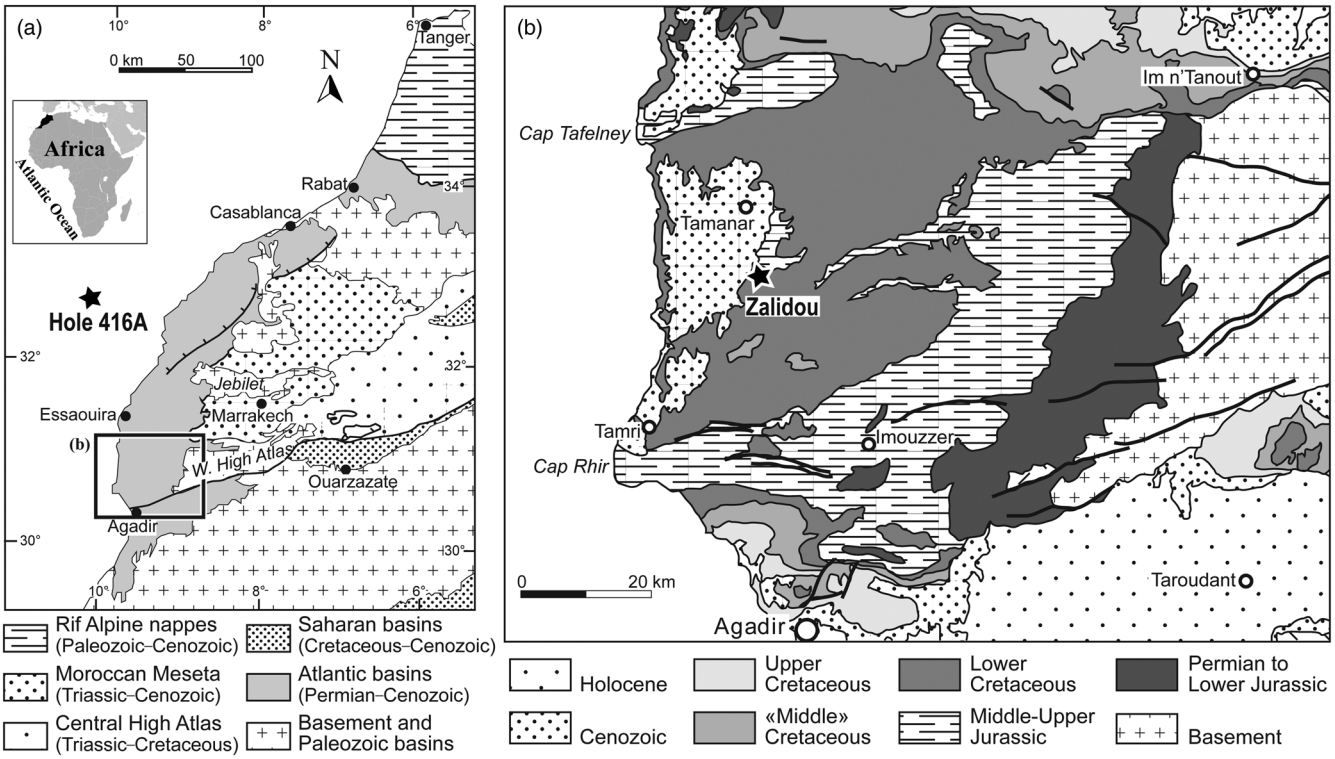

Fig. 1. Location of the study area in SW Morocco. (**a**) Location of the central Moroccan margin, including the Essaouira–Agadir Basin and DSDP Hole 416A (black star, not to scale). (**b**) Geological sketch map, including the location of the Zalidou section (black star). Source: modified from Ouajhain *et al.* (2009).

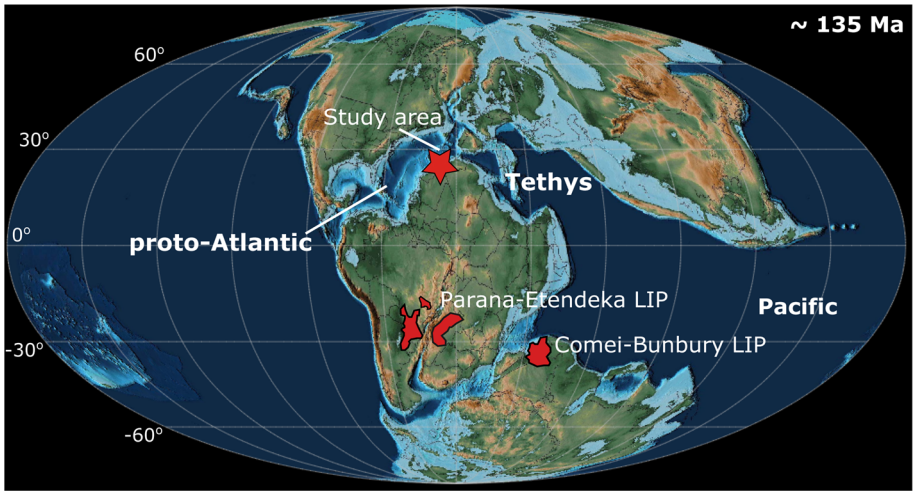

Fig. 2. Palaeogeographical map of the Valanginian (*c.* 135 Ma) showing the approximate location of the central Moroccan margin (red star). The red areas correspond to the approximate locations of the Valanginian large igneous provinces (LIPs). Source: palaeomap construction from Scotese (2016).

Zalidou section

This section is located onshore *c.* 100 km north of Agadir city (30° 54′ 23″ N; 9° 39′ 48″ W) (Fig. 1b). The rocks of Valanginian age are particularly well exposed and the lithostratigraphy and biostratigraphy (ammonites and calcareous nannofossils) have been presented by Reboulet *et al.* (2022) (Fig. S2). Briefly, the section is dated from the late Berriasian (older than 137.7 Ma, Gale *et al.* 2020) to earliest Hauterivian (younger than 132.6 Ma, Gale *et al.* 2020) and consists of an alternation of limestone and marlstone during the Valanginian stage (Fig. S2). The lower Valanginian is dominated by marlstone and thin limestone beds, whereas sandy deposits (sandy marlstone, sandy limestone and calcareous sandstone) become more common in the upper Valanginian. Traces of pyrite are observed, suggesting that reducing conditions occurred during the lower Valanginian; however, no organic-rich facies was detected. The Weissert Event interval is identified from the lower part of the *Karakaschiceras inostranzewi* to the upper part of the *Neocomites peregrinus* ammonite standard zones (upper NK3A to upper NK3B and upper CC3b to upper CC4a calcareous nannofossil subzones) (Fig. S2) (Reboulet *et al.* 2022; Shmeit *et al.* 2022).

DSDP Leg 50 Hole 416A drill core

The offshore succession was drilled *c.* 238 km NW of Zalidou (32° 50′ 10.7″ N; 10° 48′ 03.6″ W) at a water depth of 4201 m in the east Atlantic Ocean (Lancelot *et al.* 1980) (Fig. S1). The Valanginian interval is identified using calcareous nannofossils between 1542 and 1119 m b.s.f. (metres below seafloor; cores 49–9) (Čepek *et al.* 1980; Shmeit *et al.* 2022), but the uppermost Valanginian is missing (Shmeit *et al.* 2022). The lithology is described in Lancelot *et al.* (1980). Briefly, lithological unit VII (1624–1430 m b.s.f.; Fig. S2) is characterized by alternations of terrigenous and carbonate-rich turbidite cycles. The terrigenous cycles consist of fine-grained sandstone, siltstone and mudstone, whereas the carbonate-rich cycles consist of quartz-rich calcarenite, micritic limestone, siltstone and marlstone. The overlying lithological unit VI (1430–880 m b.s.f.) is characterized by distal terrigenous turbidites and differs from unit VII by the absence of micritic limestone. The cycles in lithological unit VI consist of fine sandstone, siltstone and silty mudstone, along with calcareous mudstone and marlstone. The Weissert Event interval is identified from the upper NK3A to NK3B and the CC3b to CC4a calcareous nannofossil subzones (from 1303 to 1122 m b.s.f.; Fig. S2), but part of the event is probably missing (Shmeit *et al.* 2022).

Materials and methods

We selected 20 samples from the Valanginian in the Zalidou section and 48 from DSDP Hole 416A (Fig. S2). The Zalidou samples correspond to marlstone and argillaceous limestone. For Hole 416A, the samples were collected in the most fine-grained parts of the turbiditic cycles, corresponding to marlstone and mudstone. Such fine-grained lithologies were selected to minimize the geochemical changes due to different rock types that would potentially overprint those due to changes in source/sedimentation. The Zalidou samples have a $CaCO_3$ content of *c.* 40% and Hole 416A samples have a $CaCO_3$ content between 8 and 50% (Shmeit *et al.* 2022; Supplementary Table). As a result of the scarcity of samples available in the upper Valanginian of Hole 416A, we chose samples with the highest possible $CaCO_3$ content, although this was low (<10%). All samples were finely crushed in an agate mortar for subsequent elemental and isotopic analyses.

Major and trace elements

Major elements and the loss on ignition were measured by the CNRS Service d'Analyse des Roches et des Minéraux in Nancy, France. The rock samples were digested using alkali fusion and major element analyses were carried out by flow-injection inductively coupled plasma mass spectrometry (ICP-MS) following the methods of Carignan *et al.* (2001). Accuracy was assessed based on international reference materials (BR, AN-G, UB-N, DR-N and GH; Carignan *et al.* 2001). Complete duplicate analysis of one of our samples showed a reproducibility better than 5% (Supplementary Table). The chemical index of alteration (CIA) was calculated using the molecular proportions of Al, Ca, Na and K oxides while also correcting the molar proportion of CaO for phosphate and carbonate. This correction is needed for carbonate sediments to restrict the molar proportion of CaO to that derived from silicate minerals (see Bomou *et al.* 2013 and references cited therein).

Trace element concentrations were measured at the Institut de Physique du Globe de Paris (IPGP) in Paris, France. The methods used were similar to those described in Chauvel *et al.* (2011), but with slight modifications. About 100 mg of each sample was dissolved in concentrated HNO_3 : HF using Parr bombs maintained at 150°C for more than two weeks. The only exceptions were the three basalt reference materials (BHVO-2, BR-24 and BE-N), which were digested in Savillex Teflon beakers because these reference materials do not contain refractory minerals. After dissolution, the samples were diluted using 0.5 M HNO_3 plus trace amounts of HF to reach a dilution factor of 10 000. A 5 ppb

indium standard was added to all samples prior to measurement on an Agilent 8900 inductively coupled plasma mass spectrometer. Apart from the low mass of ^{7}Li, ^{9}Be and ^{11}B, all other elements were measured in collision mode with a 5 mL min^{-1} He flux in the collision reaction cell to remove polyatomic interferences. The international reference material BE-N was used to calibrate the signal (external calibration) and was run every five to six samples during the entire sequence. The procedural blanks were negligible. The accuracy of our data as evaluated from analyses of reference rock materials (BHVO-2 and BR-24) was generally better than 5% (Supplementary Table). The precision was assessed from complete duplicate analyses of three samples that reproduced within 5% for most elements (Supplementary Table).

Radiogenic isotopes (Pb, Sr and Nd)

Chemical separations and isotopic measurements were carried out at the IPGP. The methods generally followed those described in Chauvel *et al.* (2011) after the dissolution of *c.* 50 mg of rock powder in Savillex Teflon beakers at 125°C for ten days. Procedural blanks ($n = 12$) were low (Pb < 54 pg, Sr < 100 pg and Nd < 86 pg), but there were two exceptions: one Sr blank at 770 pg and one Nd blank at 1800 pg. These two values remain negligible relative to the quantity of element in the samples and correspond to 0.016 and 1.05% of the mass isolated from the least concentrated samples of Sr and Nd, respectively. The Pb, Sr and Nd isotopic ratios were measured on a Thermo Scientific Neptune Plus multi-collector inductively coupled plasma mass spectrometer equipped with an Apex IR introductory system. The cones used for Pb and Sr were a jet sampler with an H skimmer and for Nd a jet sampler with an X skimmer. The sample flow-rate was 50 µL min^{-1}; the sample measurement time, including the wash and uptake times, was 10 min per sample. For Nd, N_2 gas was introduced into the Apex IR system at 4 bar pressure to reduce the oxides of Nd, which can form in the plasma and interfere with the signal.

The measured Sr and Nd isotope ratios were normalized to $^{88}Sr/^{86}Sr = 0.1194$ and $^{146}Nd/^{144}Nd = 0.7219$, respectively (O'Nions *et al.* 1979). For Pb measurements, the samples were spiked with Tl (5 ppb) and normalized to $^{205}Tl/^{203}Tl$ 2.38714 (White *et al.* 2000). International reference materials (NBS 981 Pb, NBS 987 Sr and AMES Rennes Nd) were measured every four samples and the average isotopic ratio of the session was used to correct for the bias relative to values published by Jochum *et al.* (2011) for Pb, by Thirlwall (1991) for Sr and by Chauvel *et al.* (2011) for Nd. Isotopic ratios measured on complete duplicate analyses of five samples and two dissolutions of the AGV-2 reference material showed that both the reproducibility and the accuracy were excellent (Supplementary Table).

The initial isotope ratios of Pb, Sr and Nd were calculated at 135 Ma to correct for radiogenic decay (equation 1; Supplementary Table).

$$\left(\frac{D}{D'}\right)_{\text{present-day}} = \left(\frac{D}{D'}\right)_{\text{initial}} + \left(\frac{P}{D'}\right)_{\text{initial}} (e^{\lambda t} - 1) \qquad (1)$$

where D is the radiogenic daughter isotope, D' is the stable isotope of the same element, P is the radioactive parent isotope, λ is the decay constant and t is the time in years.

Results

Major elements

The major element contents of the Zalidou and Hole 416A samples are reported in the Supplementary Table. The average Al_2O_3 content is higher in the Hole 416A samples (15 ± 7 wt%) than in the Zalidou samples (9 ± 5 wt%) (Fig. 3). The errors correspond to the variability between samples, calculated as two times the standard deviation of the mean. By contrast, the average SiO_2 content is slightly higher in the Zalidou samples (47 ± 15 wt%) than in the Hole 416A samples (43 ± 17 wt%). The CaO content is comparable between both successions, but shows a larger variation in the Hole 416A samples (average 11 ± 15 wt%) than in the Zalidou samples (average 17 ± 10 wt%). The studied sediments from Zalidou lie in the middle of a triangular field defined by three end-members of oceanic sediment composition (i.e. silica-rich, clay and carbonate), whereas most of the Hole 416A samples define a trend between clay and carbonate (Fig. 3).

Stratigraphic variations in the SiO_2 and CaO contents (wt%) at Zalidou show a stable trend during the entire studied interval (Fig. 4). The Al_2O_3 content shows possibly higher values (12 ± 6 wt %) in the upper part of the Weissert Event between 25.05 and 32.8 m compared with the rest of the succession (9 ± 5 wt%) (Fig. 4). Also, the calculated CIA is slightly higher (74 ± 4) in the same interval compared with the rest of the succession (68 ± 6). At Hole 416A, the SiO_2 content is steady throughout the studied interval (Fig. 4). The Al_2O_3 content increases from 11 ± 2 wt% before the Weissert Event (NK3A and upper CC3a to lower CC3b nannofossil subzones) to 16 ± 7 wt% during the Weissert Event (upper NK3A to NK3B and upper CC3b to CC4a nannofossil subzones). The CaO content is low (7 ± 8 wt%) within the Weissert Event between 1280.7 and 1187.9 m b.s.f. (upper NK3A to NK3B and upper CC3b to CC4a nannofossil subzones) compared with the rest of the succession (19 ± 15 wt%) (Fig. 4). The CIA does not vary significantly.

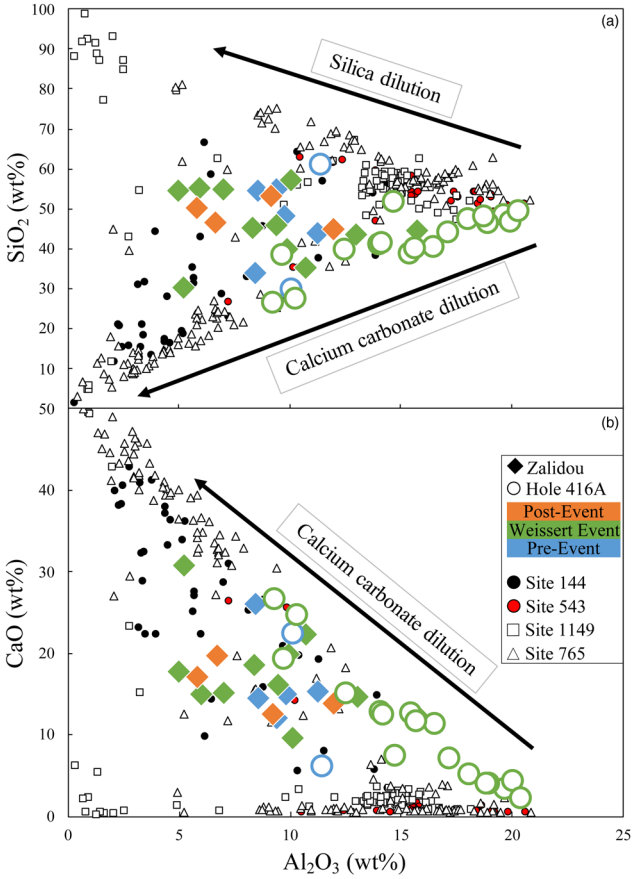

Fig. 3. (**a**) SiO_2 and (**b**) CaO v. Al_2O_3 contents (wt%) in the Zalidou and Hole 416A samples plotted before, during and after the Weissert Event. Data points are also shown from Plank *et al.* (2007) for Site 1149, Plank and Ludden (1992) for Site 765 and Carpentier *et al.* (2009) for Sites 144 and 543.

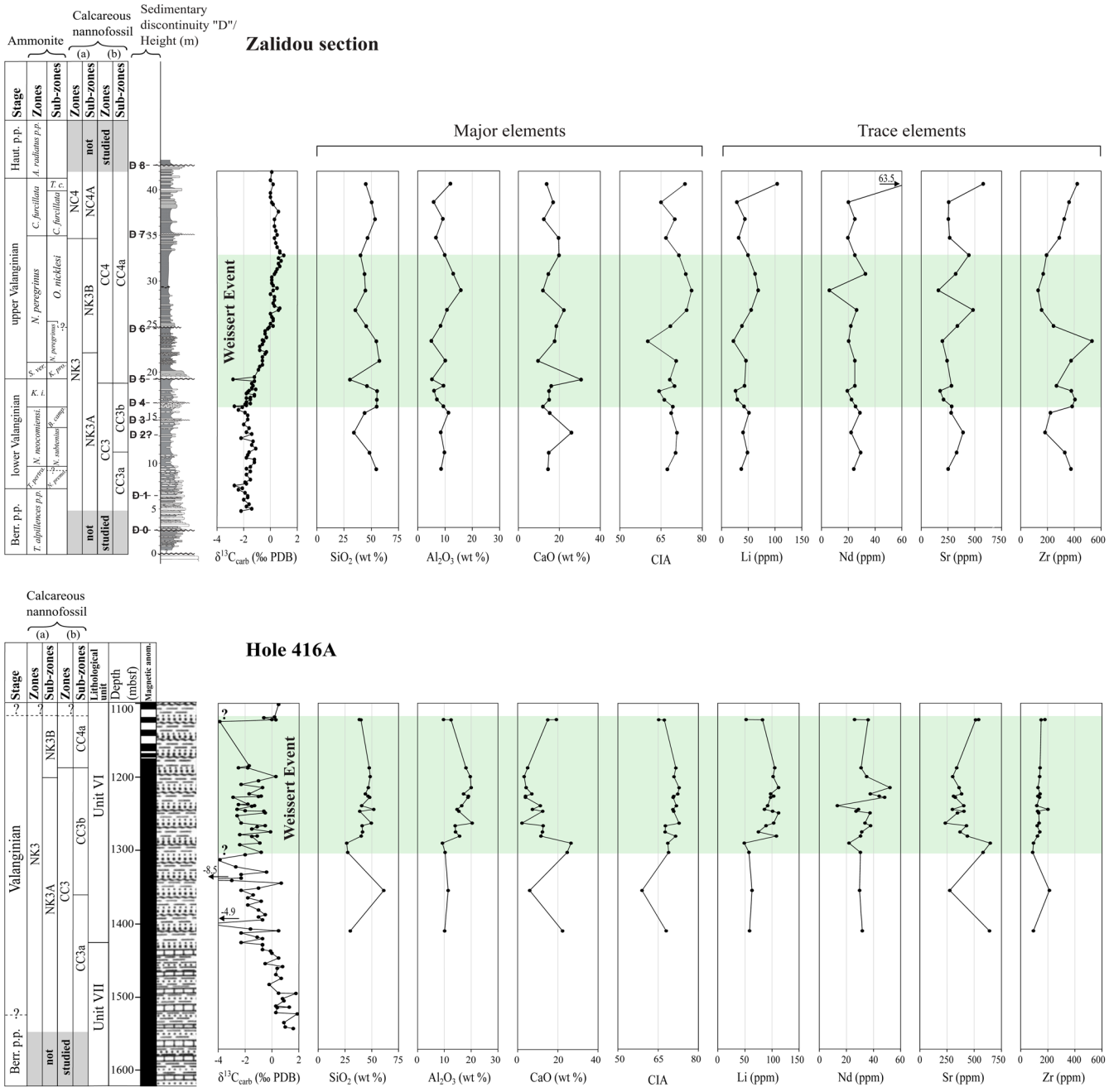

Fig. 4. Stratigraphic variations of selected major and trace elements in the Zalidou and Hole 416A samples, and of $\delta^{13}C_{carb}$ values from Shmeit *et al.* (2022). The coloured interval (green) corresponds to the Weissert Event following Shmeit *et al.* (2022). For more information on the litho- and biostratigraphy, see Fig. S2 caption. CIA, chemical index of alteration, defined as the molar ratio of $[Al_2O_3/(Al_2O_3 + CaO^* + Na_2O + K_2O)] \times 100$, with CaO* representing CaO in silicate minerals only.

Trace elements

Figure 5 shows the concentrations of Al_2O_3 v. selected trace elements, representing different oceanic sediment end-members, in the Zalidou and Hole 416A samples. Lithium, which is found in fine-grained clays, is higher in the Hole 416A samples (average 87 ± 42 ppm) than in the Zalidou samples (average 46 ± 37 ppm) (Fig. 5a). Similarly, this applies to other elements contained in clays (e.g. Cs and Rb; Supplementary Table). The rare earth element contents, the budget of which is mainly controlled by the abundance of clays, are slightly higher in the Hole 416A samples than in the Zalidou samples. For example, the concentration of Nd is higher in the Hole 416A samples (average 33 ± 17 ppm) than in the Zalidou samples (average 25 ± 2 ppm) (Fig. 5b). Strontium, which substitutes for Ca in $CaCO_3$ minerals, is higher and more variable in the Hole 416A samples (average 407 ± 239 ppm) than in the Zalidou samples (average 302 ± 215 ppm) (Fig. 5c). The high field strength elements (HFSE), mainly carried by heavy minerals present in the coarse-grained detrital sands, are significantly higher in the Zalidou samples than in the Hole 416A samples (Supplementary Table). For example, the Zr concentration is on average 302 ± 217 ppm in the Zalidou samples, but is lower (137 ± 63 ppm) in the Hole 416A samples (Fig. 5d).

The stratigraphic variations in the trace elements contained in clays and coarser grained detrital materials (Li and Nd) are stable throughout the whole studied interval at Zalidou (Fig. 4). Strontium, possibly representing a carbonate component, is also stable. The Zr concentration is consistently low (178 ± 87 ppm) in the upper part of the Weissert Event between 25.05 and 32.8 m compared with the rest of the succession (346 ± 176 ppm) (Fig. 4). This corresponds to

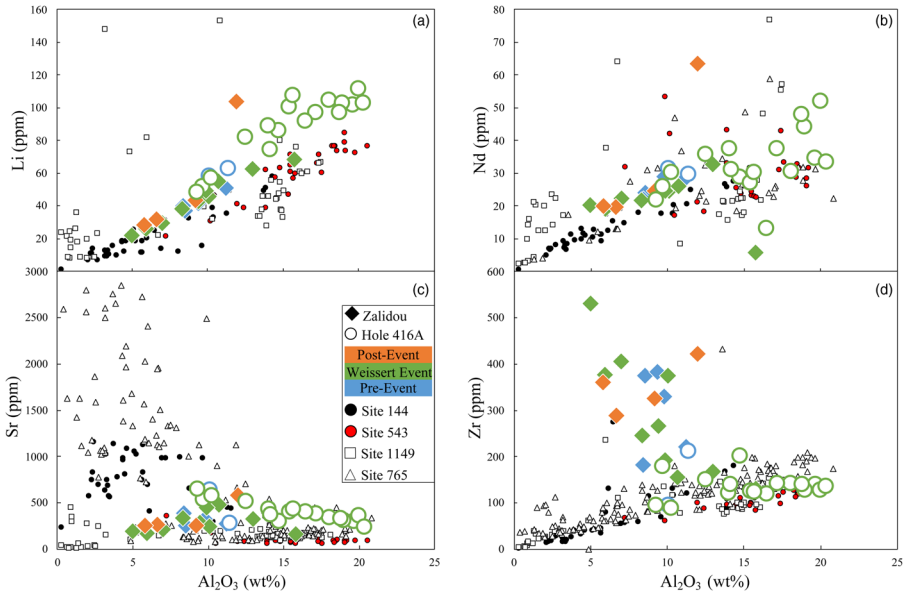

Fig. 5. Comparison of trace elements between the Zalidou and Hole 416A samples. Data points are shown from Plank *et al.* (2007) for Site 1149, Plank and Ludden (1992) for Site 765 and Carpentier *et al.* (2009) for Sites 144 and 543.

the time interval when Al_2O_3 contents are higher (*Olcostephanus nicklesi* ammonite Subzone, NK3B and CC4a nannofossil subzones; Fig. 4). At Hole 416A, the concentration of Li increases from 61 ± 7 ppm before the Weissert Event to 90 ± 40 ppm after the event (Fig. 4); this corresponds to the time interval in which the Al_2O_3 content also increases (upper NK3A to NK3B and upper CC3b to CC4a nannofossil subzones). The concentration of Nd is steady during the studied interval, although it is variable during the Weissert Event (Fig. 4). The concentrations of Sr and Zr are steady on average during the studied interval.

Radiogenic isotopes

The initial (i) and measured (m) isotopic ratios show similar stratigraphic trends, with the initial ratios consistently slightly lower than the measured ratios (Fig. 6). In the Zalidou samples, the Pb isotopic ratios are stable during the entire Valanginian stage ($^{206}Pb/^{204}Pb_{(i)}$ average 18.61 ± 0.16 and $^{208}Pb/^{204}Pb_{(i)}$ 38.68 ± 0.26, 2σ), except for the $^{207}Pb/^{204}Pb_{(i)}$ ratio, which potentially increases slightly from 15.678 ± 0.004 (2σ) before the Weissert Event to 15.683 ± 0.011 (2σ) during the event and to 15.685 ± 0.006 (2σ) after it. The Sr isotope ratios are also stable throughout the studied interval (average 0.710 ± 0.001, 2σ). However, the $^{143}Nd/^{144}Nd_{(i)}$ ratios are less variable (0.51190 ± 0.00002, 2σ) before the Weissert Event and in its lower part than in the rest of the succession (0.51190 ± 0.00004, 2σ) (Fig. 6). Two outliers have different Pb initial isotope ratios in the Zalidou section (sample Za 51b at 28.95 m and sample Za 56a at 40.6 m; Fig. 6). Sample Za 51b has a low $^{206}Pb/^{204}Pb_{(i)}$ ratio and a high $^{208}Pb/^{204}Pb_{(i)}$ ratio due to its high U/Pb and low Th/Pb ratios (Supplementary Table). Sample Za 56a has a low $^{208}Pb/^{204}Pb_{(i)}$ ratio because of its high Th/Pb ratio. We suspect that these anomalous ratios are due to recent events and are unrelated to the original contents, resulting in an overcorrection with age.

In the Hole 416A samples, the Pb isotopic ratios are steady during the Valanginian stage ($^{206}Pb/^{204}Pb_{(i)}$ average 18.68 ± 0.15; $^{207}Pb/^{204}Pb_{(i)}$ 15.69 ± 0.02; $^{208}Pb/^{204}Pb_{(i)}$ 38.73 ± 0.15, 2σ). The Sr isotopic ratios are highly variable (average 0.7106 ± 0.0027, 2σ) and do not show any significant trend. The Nd isotopic ratios are moderately constant (average 0.51190 ± 0.00007, 2σ). The $^{143}Nd/^{144}Nd_{(i)}$ ratios show minor variations (0.51187 ± 0.00003, 2σ) during the Weissert Event (between 1263 and 1188 m b.s.f.; upper NK3A to lower NK3B and upper CC3b nannofossil subzones) than during the rest of the studied time interval (0.51191 ± 0.00007, 2σ).

The $^{206}Pb/^{204}Pb_{(i)}$ and $^{207}Pb/^{204}Pb_{(i)}$ ratios are similar at the two sites (Fig. 7a). However, the $^{208}Pb/^{204}Pb_{(i)}$ ratios are slightly higher in the Hole 416A samples than in the Zalidou samples, such that the majority of the Hole 416A samples have $^{208}Pb/^{204}Pb_{(i)} > 38.75$, whereas the Zalidou samples have ratios <38.75 (Fig. 7b). The $^{87}Sr/^{86}Sr_{(i)}$ isotopic ratios are on average slightly higher and more variable in the Hole 416A samples than in the Zalidou samples; some samples from Hole 416A have $^{87}Sr/^{86}Sr_{(i)} > 0.7106$ (Fig. 7c). By contrast, all samples from Zalidou have ratios <0.7106. The $^{143}Nd/^{144}Nd_{(i)}$ ratios are similar in both successions (Fig. 7d).

Discussion

The positive CIE corresponding to the Weissert Event (Valanginian stage, 137.7–132.6 Ma) is mainly interpreted as the consequence of enhanced marine primary productivity (Lini *et al.* 1992; Bartolini 2003; Erba *et al.* 2004). Multiple micropalaeontological (e.g. Bersezio *et al.* 2002; Duchamp-Alphonse *et al.* 2007; Bornemann and Mutterlose 2008; Mattioli *et al.* 2014) and geochemical (e.g. Plank *et al.* 2000; Bartolini 2003; Morales *et al.* 2015) studies support increasing marine primary productivity and fertility during the Valanginian stage.

An increase in marine primary productivity requires enhanced nutrification and there are two main hypotheses: higher continental weathering rates and/or intensified oceanic upwelling (Lini *et al.* 1992; Föllmi *et al.* 1994; Erba *et al.* 2004). These two processes would have different impacts in proximal and distal marine settings. Comparing the time evolution of the two types of settings could therefore help us to understand the cause(s) of increasing productivity. Enhanced continental weathering and hydrolysing conditions during the Valanginian stage are demonstrated by the clay mineral assemblages (Westermann *et al.* 2013; Charbonnier *et al.* 2020), spore–pollen ratios (Kujau *et al.* 2013) and sediment enrichments in continentally sourced elements (Al, Mn, Fe and P; Van De Schootbrugge *et al.* 2003; Kuhn *et al.* 2005; Duchamp-Alphonse *et al.* 2007; Morales *et al.* 2015).

Continental weathering ultimately increases the nutrient input in proximal marine settings close to areas of fluvial discharge. A substantial input of nutrients from the continent would therefore result in a crustal geochemical signature in the central Moroccan margin sediments, particularly in the proximal setting (Zalidou),

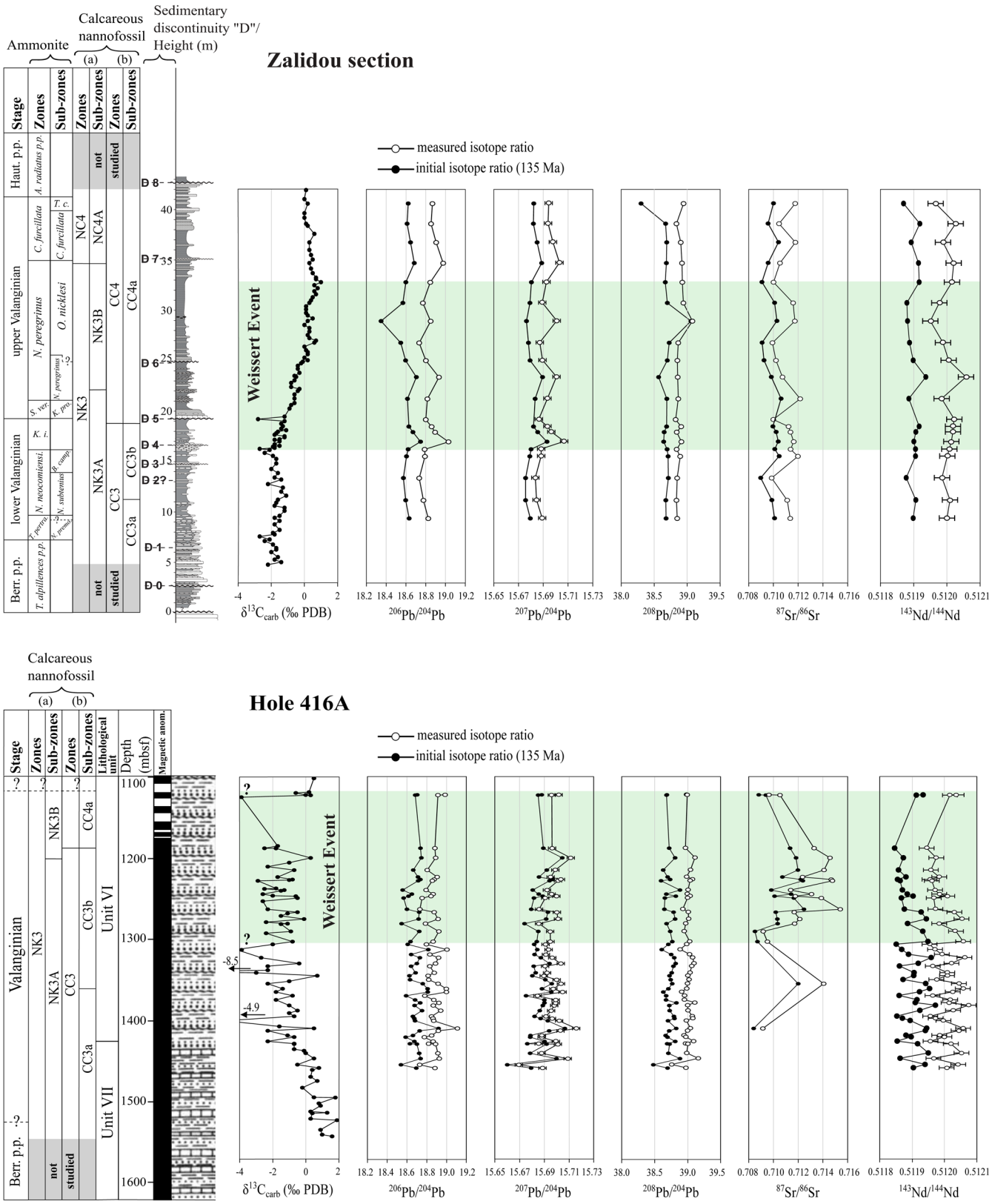

Fig. 6. Stratigraphic variations in measured and initial isotope ratios of Pb, Sr and Nd in Zalidou and Hole 416A samples (see Supplementary Table). Error bars on measured isotopic ratios are assessed from analytical measurements of the international reference materials. The coloured interval (green) corresponds to the Weissert Event following Shmeit *et al.* (2022); see also caption of Fig. S2. Initial isotope ratios are calculated at 135 Ma using the decay constants and the half-life of parent/daughter decay systems from Villa *et al.* (2015) for Rb–Sr, Jaffey *et al.* (1971) and Le Roux and Glendenin (1963) for U–Th–Pb and Villa *et al.* (2020) for Sm–Nd.

which is closer to inputs from rivers. By contrast, the upwelling of nutrient-rich deep waters should increase nutrient levels in pelagic settings (Bartolini 2003; Erba *et al.* 2004; Föllmi 2012). Existing evidence includes abundance peaks in the radiolarian taxa *Pantanellium* in the Tethys and Pacific realms (Jud 1994; Bartolini 2003). The presence of steryl ethers in the Pacific Ocean may be a biomarker of cool water, high seasonal productivity and/or nutrient input by upwelling (Brassell 2009). A significant input of

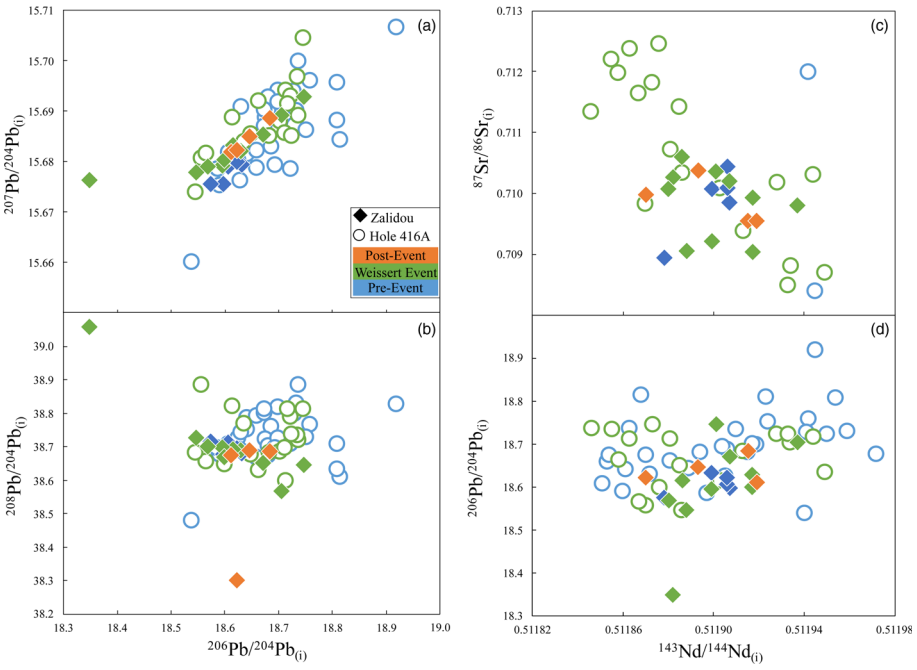

Fig. 7. Comparison of the initial (i) isotope ratios at 135 Ma of Pb, Sr and Nd between the Zalidou and Hole 416A samples.

nutrients from upwelling on the central Moroccan margin should enhance an oceanic crust signature in the sediments and should be more pronounced in the distal setting (Hole 416A), which is closer to possible oceanic upwelling.

Was there any geochemical change on the central Moroccan margin during the Weissert Event?

In the proximal Zalidou section, the steady stratigraphic trends in the selected major element contents (Al_2O_3, SiO_2 and CaO) support the view that continental weathering and the input of detrital material, from both coarse- and fine-grained minerals, was stable throughout the Valanginian stage (Fig. 4). The trace elements associated with detrital and continental sources (e.g. Li and Nd) also display a steady trend (Fig. 4), supporting an almost continuous weathering and hydrolysis regime. However, the consistently low concentrations of HFSE (i.e. Zr and Hf) in the upper part of the Weissert Event (between 25.05 and 32.8 m, *O. nicklesi* ammonite Subzone, NK3B and CC4a nannofossil subzones; see Fig. 4 and Supplementary Table) suggest the low deposition of coarse-grained clastics (i.e. quartz). This may be related to the sandy marlstones (fine-grained lithology) of this interval, which were deposited under conditions of sea-level rise (maximal flooding; Reboulet *et al.* 2022). The calculated CIA is generally steady, further supporting a constant rate of hydrolysis on the continent. The slightly higher values at the same level at which HFSE have low concentrations might reflect higher contents of fine-grained material, such as aluminosilicates, related to the deeper depositional setting. The unchanged Pb, Sr and Nd isotopic ratios do not support any geochemical change during the Valanginian stage (Fig. 6).

In the distal Hole 416A, the stable SiO_2 content and CIA suggest, respectively, a steady input of coarse-grained clastic material and a constant rate of hydrolysis for the studied Valanginian interval (Fig. 4). However, the increasing Al_2O_3 content suggests a higher input of fine-grained detrital material within the Weissert Event (from 1280.71 to 1187.94 m b.s.f., upper NK3A to NK3B and upper CC3b to CC4a nannofossil subzones). A concomitant reduction in carbonate deposition is also suggested by the decreasing CaO content. Such changes are evident at the beginning of the Weissert Event within lithological unit VI. In the lower part of that unit, two calcareous and quartz-rich turbidite cycles are recognized, whereas the cycles in its upper part are uniform and grade from sandstone to marlstone and claystone (Lancelot *et al.* 1980). The level of this lithological change is not certain, occurs gradually and was first recorded at *c.* 1299 m b.s.f. (core 22). In addition, the increase in the Li concentration during the Weissert Event (upper NK3A to NK3B and upper CC3b to CC4a nannofossil subzones) complements the observation from the major elements (Fig. 4) because the proportion of clays controls the Li content. The input of continental and coarse-grained clastics was probably steady, as observed from the uniform HFSE and rare earth element contents (Fig. 4; Supplementary Table). The Pb, Sr and Nd isotopic ratios do not show any significant change throughout the studied Valanginian interval (Fig. 6); even if inter-sample variations in Sr and Nd are observed, they are most probably related to the increase in clay mineral deposition during the Weissert Event.

In summary, there is no significant change in the sediment major and trace element concentrations on the central Moroccan margin during the Valanginian stage. The few stratigraphic variations in major and trace element concentrations are most probably caused by variations in sediment lithology, with a higher clay input and lower detrital quartz input during the upper part of the Weissert Event in Zalidou and within the identified Weissert Event interval in Hole 416A. Similarly, the radiogenic isotopes Pb, Sr and Nd do not show any significant trend during the Valanginian stage, suggesting no major change in the source material during the event.

How do the sediments from proximal and distal sites compare?

The distal Hole 416A shows a simple binary mixture of clay and carbonate sediments. By contrast, the proximal Zalidou section shows a more complex mixture of detrital deposits with a continental origin (silica-rich and clay) and carbonates. This complexity is illustrated by the distribution of the major elements (Fig. 3). The Hole 416A sediments are relatively rich in Al-rich components, such as fine-grained clays (i.e. aluminosilicates). The Zalidou sediments are relatively rich in coarse-grained Si-rich

components (i.e. quartz), as shown by the slightly higher SiO_2 content. It is noteworthy that the analysed samples correspond to fine-grained lithologies as we avoided sampling coarse-grained sediments. The observed difference between sites (proximal v. distal) is caused by the different depositional settings. Clays are lightweight minerals and can travel further and accumulate in deeper settings (e.g. Hole 416A). By contrast, coarse-grained clastic minerals are heavy and accumulate in proximal settings close to the output of rivers (e.g. Zalidou).

Differences in the concentrations of trace elements between the Zalidou and Hole 416A samples also highlight their different depositional settings. The higher concentrations of Li in the Hole 416A samples reflect the more significant proportion of clays compared with the Zalidou samples (Fig. 5a) because Li is concentrated in fine-grained minerals rather than coarse-grained minerals (Sauzéat *et al.* 2015 and references cited therein). Lithium could also reflect a higher proportion of authigenic clay minerals in the Hole 416A samples rather than detrital clays (see Andrews *et al.* 2020 and references cited therein). The concentration of Nd is marginally higher in the Hole 416A samples than in the Zalidou samples, indicating that both successions record input from continental detrital material. The high Zr concentrations in the Zalidou samples compared with the Hole 416A samples (Fig. 5d) are explained by its proximal depositional setting close to the fluvial input of coarse clastic minerals. Zirconium, like other HFSE, resides in heavy minerals such as zircon, minerals that are not transported far in a basin and are deposited close to the continental margin (Patchett *et al.* 1984). By contrast, fine-grained (lightweight) clays deposited further away from the continent show deficiencies in Zr and Hf.

The initial isotope ratios of Pb, Sr and Nd are comparable between both studied successions, but with a few differences. The slightly more radiogenic $^{208}Pb/^{204}Pb_{(i)}$ and $^{87}Sr/^{86}Sr_{(i)}$ ratios in the Hole 416A samples than in the Zalidou samples can be explained by a contribution from a source of more radiogenic sediments (Fig. 7b, c). In summary, the geochemical differences observed between the two studied successions relate mainly to their depositional setting (proximal v. distal) and to the associated chemical fractionation occurring during the transport of sediments.

Is there a volcanic input during the Weissert Event?

The environmental perturbations discussed in previous sections are tentatively linked to extensive volcanism from the Paraná–Etendeka LIP of South America–SW Africa (Weissert *et al.* 1998; Erba *et al.* 2004) or the Comei–Bunbury LIP of SE Tibet–SW Australia (Zhu *et al.* 2009). Uncertainties related to age models (e.g. the scarcity of data, uncertainty in age models and in the absolute age calibration) hinder direct temporal correlation between these LIPs and the Weissert Event (Charbonnier *et al.* 2017). The radiometric ages of basalts from the Paraná–Etendeka LIP (135.5–126 Ma; e.g. Thompson *et al.* 2001; Trumbull *et al.* 2004; Almeida *et al.* 2018; Baksi 2018; Rocha *et al.* 2020; Bacha *et al.* 2022) and the Comei–Bunbury LIP (134–123 Ma; e.g. Zhu *et al.* 2008, 2009; Liu *et al.* 2015) probably post-date the onset of the Valanginian positive CIE (135.22 ± 1.0 Ma; Martinez *et al.* 2015). Moreover, Charbonnier *et al.* (2017) observed Hg enrichments interpreted as volcanic in origin in sediments at or near the onset of the Weissert Event from the Central Tethys. Fesneau *et al.* (2009) observed an ochre-coloured layer of lower Valanginian age in the Vocontian Basin (France) enriched in trace elements with a specific magmatic affinity (Zr, Ba, Th, Y, Hf, U, Pb, Nb and Ta). The layer was interpreted as 'bentonite' of volcanic origin.

These studies cannot designate unambiguously if one or both of the LIPs was involved in the Weissert Event. Chavagnac *et al.* (2008) and Peate (2009) observed overlapping Pb isotopic compositions from Hole 1149B and magmas from the Paraná–Etendeka LIP. The majority of samples that show a Pb isotopic shift in the Hole 1149B samples (upper lithological unit IV; cores 20R–16R) belong to the Hauterivian stage (Lozar and Tremolada 2003) and the Nd/Sr isotope ratios were not compared with the LIPs. Using a combination of Pb, Sr and Nd isotopes should constrain the relationship between either of these two LIPs and the Weissert Event. For example, a volcanic contribution to the sediments is expected to cause a more radiogenic Nd isotopic composition (i.e. radiogenic mantle source) and less radiogenic Sr and Pb isotope ratios.

The Nd isotopic composition in both studied successions on the central Moroccan margin does not increase to more radiogenic ratios (Fig. 6). Figure 8 compares the initial isotope ratios (135 Ma) of Pb,

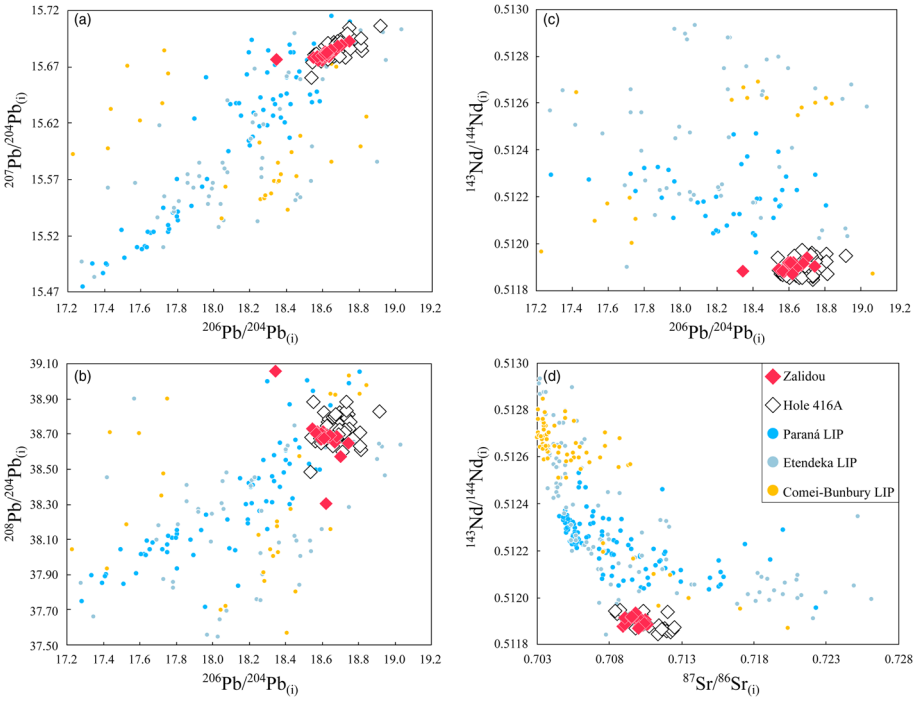

Fig. 8. Comparison of the initial isotope ratios at 135 Ma in the central Moroccan margin sediments with Early Cretaceous large igneous provinces. References for the isotope ratios of the large igneous provinces (see also Supplementary Table): Paraná basalts (Hawkesworth *et al.* 1986; Peate and Hawkesworth 1996; Marques *et al.* 1999, 2018; Peate *et al.* 1999; Turner *et al.* 1999; Rocha-Júnior *et al.* 2013; Barreto *et al.* 2016; Rämö *et al.* 2016); Etendeka basalts (Ewart *et al.* 1998*a*, 2004*a*; Le Roex and Lanyon 1998; Mingram *et al.* 2000; Thompson *et al.* 2001); Etendeka silicic sequences (Ewart *et al.* 1998*b*, 2004*b*; Trumbull *et al.* 2004); Comei basalts (Zhu *et al.* 2008; Liu *et al.* 2015); and Bunbury basalt and silicic sequences (Ewart *et al.* 1992; Frey *et al.* 1996; Allen *et al.* 1997; Direen *et al.* 2017). LIP, large igneous province.

Sr and Nd obtained on the central Moroccan margin sediments with those published for the suggested Valanginian LIPs. The Pb and Sr isotopic ratios of the sediments overlap with the higher ratios reported for the Paraná–Etendeka LIP at $^{206}Pb/^{204}Pb_{(i)} > 18.5$, $^{207}Pb/^{204}Pb_{(i)} > 15.66$, $^{208}Pb/^{204}Pb_{(i)} > 38.5$ and $^{87}Sr/^{86}Sr_{(i)} > 0.708$. However, the Nd isotopic ratios are lower in the central Moroccan margin sediments ($^{143}Nd/^{144}Nd_{(i)} < 0.5120$) than in any of the LIPs ($^{143}Nd/^{144}Nd_{(i)} > 0.5120$) shown in Figure 8d. This difference is a strong argument against a significant input of volcanic material from the LIPs to sediments on the central Moroccan margin during the Valanginian stage.

Continental runoff v. upwelling causing eutrophication

Figure S3 shows the trace element patterns of the Zalidou and Hole 416A samples normalized to the upper continental crust (UCC) values of Rudnick and Gao (2013). The studied successions show trace element patterns similar to the UCC for the majority of elements. This similarity suggests that the sediment trace element budget is controlled by material with a continental origin. The few element enrichments/depletions relative to the UCC are caused by the chemical fractionation of elements during sediment transport (see Fig. S3 caption). As a consequence, the trace element patterns of the Hole 416A bulk sediment samples exclude the possibility of a significant role for the input of nutrients from oceanic upwelling in the composition of the deposits. The Hole 416A sediments have a chemical signature primarily controlled by terrigenous input. Indeed, the sedimentation rate in Hole 416A is high (65 m myr^{-1}) and the sediments are dominated by detrital material (Lancelot *et al.* 1980). Carpentier *et al.* (2013) showed that offshore settings close to continental shelves have a chemical composition (signature) similar to the nearby continental source areas. Alternatively, the oceanic and atmospheric conditions during the Valanginian did not induce significant upwelling on this part of the Moroccan margin.

Our new isotope results also support the view that upwelling did not contribute significantly to the Hole 416A sediments. In principle, strong upwelling should induce a juvenile oceanic crust isotopic signature in the sediments. However, this is not the case at Hole 416A. First, the Pb and Sr isotopic ratios of Hole 416A sediments are very similar to those of the Zalidou proximal sediments, supporting the interpretation that they were fed by the same continental source (Fig. 7). Second, the average ε_{Nd} values in the two studied successions are identical (*c.* -12 ± 1; Supplementary Table) and of continental origin, even lower than the average UCC value (-10.3 ± 1.2, 1σ) reported by Chauvel *et al.* (2014). These similar values further support a common continental source for the Zalidou and Hole 416A sediments and undermine a significant contribution to the sediments from upwelling.

What is the source of the central Moroccan margin sediments?

The Pb, Sr and Nd isotopic compositions of the central Moroccan margin sediments are dominated by continental material. It is therefore worth comparing the isotopic composition of sediments to what is known for the surrounding crustal areas exposed during the Valanginian to establish the source area(s). Lead and Nd isotopes are particularly useful in this respect because model ages can be calculated for both isotopic systems. Such model ages do not provide a precise measure of the age of the eroded material. However, they estimate the average age of formation of the material eroded from the continental crust. The slope defined by the central Moroccan margin sediments in a $^{206}Pb/^{204}Pb_{(m)}$ v. $^{207}Pb/^{204}Pb_{(m)}$ isotopic space (Fig. S4 and its caption) provides an average model age of *c.* 1.1 Ga for the source of the sediments. By contrast, the Nd isotopes provide a model age of *c.* 1.9 Ga when using the parameters from Chauvel *et al.* (2008, 2014). Both isotopic systems therefore suggest that the central Moroccan margin was fed by sediments from an old and continental cratonic source. The source of sediments did not change during the Valanginian stage, as observed from the unchanged isotopic ratios of Pb, Sr and Nd (Fig. 6).

The best approach to trace the origin of sediments deposited in the basin is to compare the isotopic compositions of sediments and potential sources in the area. We measured the Pb, Sr and Nd isotopes in the sediments, but studies of potential sources reporting data for the combined three isotopic systems are limited. We therefore considered only the Nd and Sr isotopes in Figure 9 because they are the only two isotopic systems for which there is an extensive database. Because most published data on the potential sources do not report the parent–daughter isotope ratios, we calculated their initial isotope ratios at 135 Ma (Supplementary Table) using the recommended Sm/Nd and Rb/Sr ratios for the UCC (Rudnick and Gao 2013). Given that these terranes are old crustal materials, this should not be a problem.

In the Sr–Nd space of Figure 9, the central Moroccan margin sediments overlap with the African dust sources (Sahara region; Fig. S5), both having $^{143}Nd/^{144}Nd_{(i)}$ ratios clustering between 0.5118 and 0.5120. The Sr isotopic composition of the African dust sources is highly variable and generally more radiogenic than that of the central Moroccan margin sediments (Fig. 9), but this is probably because the fine size of the dust particles means that they are naturally more concentrated in Rb-rich clays, which consequently have more radiogenic Sr isotope ratios. The studied sediments lie in between two additional end-members: (1) the West African Craton (2.1 Ga) (Fig. S5); and (2) the surrounding Moroccan massifs, such as the NE Meseta (344 Ma), Anti-Atlas (560–543 Ma) and the central Jebilet (240 Ma) massifs (Fig. 9 and Fig. S5). The contribution of sediments via fluvial input from both of these 'cratonic' end-members is highly plausible considering their geographical proximity to the studied successions. It is noteworthy that the Jebilet massif and the Anti-Atlas are closer to the Zalidou section (see Fig. 1a and Fig. S5), whereas the Moroccan Meseta is closer to Hole 416A (Fig. S5).

The slightly more radiogenic Pb and Sr ratios observed in the Hole 416A samples than in the Zalidou samples (Fig. 7b, c) might have their origin in a relatively less important contribution from a fluvial input in the offshore succession, resulting in a more significant signature of the dust component. Figure S6 compares the initial Pb and Sr isotope ratios of the Zalidou and Hole 416A sediments with surrounding areas for which data exist for these isotopic systems and suggests that the distant African Sahara regions (the Saharan metacraton and Sahel Desert; Fig. S5) could cause such a shift to more radiogenic Pb and Sr isotopic ratios. Nonetheless, surface winds blew SW over north Africa during the Cretaceous (Poulsen *et al.* 1998), so the relatively northward Hole 416A should hypothetically receive less dust input (see Fig. 1a and Fig. S5). Accordingly, fluvial input from other massifs more proximal to Hole 416A (e.g. the middle Atlas) could have caused this difference, but we cannot test for their contribution due to the lack of isotope studies.

In summary, the isotopic signature of the central Moroccan margin sediments is dominated by old continental sources. The African Sahara regions could have significantly contributed to the central Moroccan margin sediments through wind transport. Today, the Sahara and north African terranes are known as the most important sources of dust to the Atlantic Ocean (e.g. Grousset and Biscaye 2005; Abouchami *et al.* 2013). During the Valanginian stage (137.7–132.6 Ma), dust input from old African terranes located to the east could be similarly expected. Indeed, the wind circulation models of Price *et al.* (1995) show west and SW wind vectors over north Africa in the Jurassic and Cretaceous. The

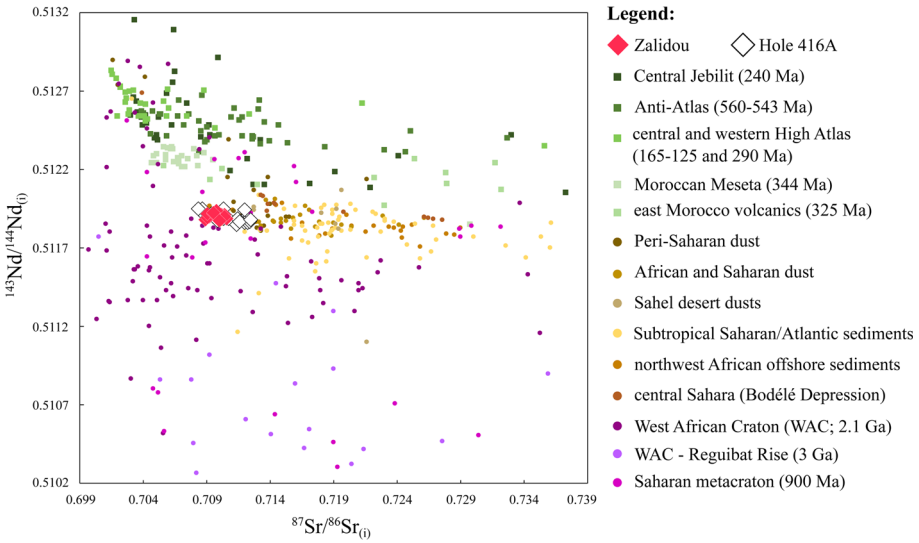

Fig. 9. Comparison of the initial isotope ratios of the central Moroccan margin sediments with surrounding possible source areas with data for only Sr and Nd isotopes. Green symbols, Moroccan massifs; yellow symbols, African and Saharan dust sources; and purple symbols, West African Craton. Data references (see also Supplementary Table): Central Jebilet 240–330 Ma (Essaifi *et al.* 2014; Bouloton *et al.* 2019), Anti-Atlas 543–560 Ma (Toummite *et al.* 2013; Belkacim *et al.* 2017), Central High Atlas 165–125 Ma (Essaifi and Zayane 2018), Western High Atlas 290 Ma (Gasquet *et al.* 1992), NE Meseta 344 Ma (Ajaji *et al.* 1998) and east Morocco complex including the El Jadida complex (Chalot-Prat 1995; Gasquet *et al.* 2005; EL Haibi *et al.* 2020); Holocene Peri-Saharan dust (Grousset *et al.* 1992), modern African and Saharan dust (Grousset and Biscaye 2005; Skonieczny *et al.* 2013; Gross *et al.* 2016), modern Sahel desert dusts (Kumar *et al.* 2014), modern and Holocene subtropical Saharan/Atlantic sediments (Grousset *et al.* 1998; Meyer *et al.* 2011) and the central Sahara Bodélé Depression (Abouchami *et al.* 2013); and West African Craton 2.1 Ga (Boher *et al.* 1992; Pawlig *et al.* 2006; Tapsoba *et al.* 2013), 2.9 Ga West African Craton and Reguibat Rise (Blanc *et al.* 1992; Peucat *et al.* 1996, 2005; Bea *et al.* 2013; Montero *et al.* 2014) and 900 Ma Saharan metacraton (Küster *et al.* 2008).

surrounding Moroccan massifs could also have contributed to the sediments via direct fluvial transport.

Conclusions

Valanginian carbonate deposits from two geological successions on the central Moroccan margin show geochemical signatures characteristic of their respective depositional settings (proximal v. distal). The onshore Zalidou section consists of a mixture of detrital (silica-rich and clay) and carbonate materials, whereas the offshore DSDP Hole 416A section shows a binary mixture of clay and carbonate. The major and trace elements show a higher coarse-grained detrital input (silica-rich) in the Zalidou section and a higher authigenic clay input (aluminosilicates) in Hole 416A. This is a result of mineral sorting processes occurring during the transport of sediments, leading to the chemical fractionation of some elements. Nonetheless, the similar radiogenic isotope signature between both sites suggests a common 'old' and continental source for all the sediments. No trace of a significant input from oceanic upwelling can be detected in the distal site sediments. This suggests that the central Moroccan margin was primarily fed by nutrients from continental runoff and weathering before, during and after the Weissert Event. The source of sediments also did not change throughout the studied Valanginian interval and was most probably the African Sahara regions.

No volcanic contribution from the Paraná–Etendeka or the Comei–Bunbury LIPs was detected in the sediments during the entire Valanginian stage. If any such material reached the central Moroccan margin, the quantities must have been small enough to not modify the dominantly continental signature of the sediments. It cannot be excluded that volcanic material might have affected the seawater without changing the composition of the deposited sediments during the Weissert Event. It is therefore difficult to imagine that the LIPs triggered the Weissert Event recorded in the studied area. Our study shows the potential of combining several radiogenic isotopes to test for a volcanic contribution in sediments during the Weissert Event and to identify the specific LIP that was involved.

Acknowledgements Pamela Gutiérrez, Pascale Louvat and Pierre Burckel are warmly thanked for their help in the chemistry laboratory and for their assistance during the inductively coupled plasma mass spectrometry measurements. We are grateful to the Editor Kirsty Marie Edgar and two anonymous reviewers for their corrections and comments, which greatly improved the quality of an earlier version of this paper.

Author contributions **MS**: conceptualization (lead), formal analysis (lead), funding acquisition (supporting), investigation (lead), methodology (lead), project administration (equal), resources (supporting), software (lead), supervision (equal), validation (lead), visualization (lead), writing – original draft (lead), writing – review & editing (lead); **CC**: conceptualization (equal), formal analysis (equal), funding acquisition (equal), investigation (equal), methodology (equal), project administration (equal), resources (equal), supervision (lead), validation (equal), visualization (equal), writing – original draft (equal), writing – review & editing (equal); **FG**: conceptualization (equal), formal analysis (supporting), funding acquisition (lead), investigation (equal), project administration (equal), resources (lead), supervision (supporting), validation (supporting), visualization (supporting), writing – original draft (supporting), writing – review & editing (supporting); **EJ**: conceptualization (equal), formal analysis (supporting), investigation (equal), supervision (supporting), validation (supporting), visualization (supporting), writing – original draft (supporting), writing – review & editing (supporting); **SR**: conceptualization (supporting), formal analysis (supporting), investigation (supporting), supervision (supporting), validation (supporting), writing – review & editing (supporting); **MM**: investigation (equal); **JES**: investigation (supporting), writing – original draft (supporting), writing – review & editing (supporting); **AE-S**: writing – original draft (supporting), writing – review & editing (supporting).

Funding This work benefited from financial support from the Ministries of Foreign Affairs of France and Morocco (PHC Project No. 031/STU/13), the French IRD, Campus France and various grants from ISTerre, the Laboratoire de Géologie de Lyon, the OSUG@2020 Labex, the CNRS SYSTER program and IODP France Soutien post-cruise.

Competing interests The authors declare that they have no known competing financial interests or personal relationships that could have appeared to influence the work reported in this paper.

Data availability All data generated or analysed during this study are included in this published article (and its Supplementary information files).

Scientific editing by Kirsty Edgar

References

Abouchami, W., Näthe, K. *et al.* 2013. Geochemical and isotopic characterization of the Bodélé Depression dust source and implications for transatlantic dust transport to the Amazon basin. *Earth and Planetary Science Letters*, **380**, 112–123, https://doi.org/10.1016/j.epsl.2013.08.028

Aguado, R., Company, M., Castro, J.M., de Gea, G.A., Molina, J.M., Nieto, L.M. and Ruiz-Ortiz, P.A. 2018. A new record of the Weissert episode from the Valanginian succession of Cehegín (Subbetic, SE Spain): bio- and carbon isotope stratigraphy. *Cretaceous Research*, **92**, 122–137, https://doi.org/10.1016/j.cretres.2018.07.010

Aguirre-Urreta, M.B., Price, G.D., Ruffell, A.H., Lazo, D.G., Kalin, R.M., Ogle, N. and Rawson, P.F. 2008. Southern hemisphere Early Cretaceous (Valanginian–Early Barremian) carbon and oxygen isotope curves from the Neuquén Basin, Argentina. *Cretaceous Research*, **29**, 87–99, https://doi.org/10.1016/j.cretres.2007.04.002

Ajaji, T., Weis, D., Giret, A. and Bouabdellah, M. 1998. Coeval potassic and sodic calc-alkaline series in the post-collisional Hercynian Tanncherfi intrusive complex, northeastern Morocco: geochemical, isotopic and geochronological evidence. *Lithos*, **45**, 371–393, https://doi.org/10.1016/S0024-4937(98)00040-1

Allen, C.M., Wooden, J.L. and Chappell, B.W. 1997. Late Paleozoic crustal history of central coastal Queensland interpreted from geochemistry of Mesozoic plutons: the effects of continental rifting. *Lithos*, **42**, 67–88, https://doi.org/10.1016/S0024-4937(97)00037-6

Almeida, V.V., Janasi, V.A., Heaman, L.M., Shaulis, B.J., Hollanda, M.H.B.M. and Renne, P.R. 2018. Contemporaneous alkaline and tholeiitic magmatism in the Ponta Grossa Arch, Paraná–Etendeka magmatic province: constraints from U–Pb zircon/baddeleyite and $^{40}Ar/^{39}Ar$ phlogopite dating of the José Fernandes Gabbro and mafic dykes. *Journal of Volcanology and Geothermal Research*, **355**, 55–65, https://doi.org/10.1016/j.jvolgeores.2017.01.018

Andrews, E., Pogge von Strandmann, P.A.E. and Fantle, M.S. 2020. Exploring the importance of authigenic clay formation in the global Li cycle. *Geochimica et Cosmochimica Acta*, **289**, 47–68, https://doi.org/10.1016/j.gca.2020.08.018

Arthur, M.A., Brumsack, H.J., Jenkyns, H.C. and Schlanger, S.O. 1990. Stratigraphy, geochemistry, and paleoceanography of organic carbon- rich Cretaceous sequences. *NATO ASI Series*, **304**, 75–119, https://doi.org/10.1007/978-94-015-6861-6_6

Bacha, R.R., Waichel, B.L. and Ernst, R.E. 2022. The mafic volcanic climax of the Paraná-Etendeka large igneous province as the trigger of the Weissert event. *Terra Nova*, **34**, 28–36, https://doi.org/10.1111/ter.12558

Baksi, A.K. 2018. Paraná flood basalt volcanism primarily limited to *c.* 1 Myr beginning at 135 Ma: new $^{40}Ar/^{39}Ar$ ages for rocks from Rio Grande do Sul, and critical evaluation of published radiometric data. *Journal of Volcanology and Geothermal Research*, **355**, 66–77, https://doi.org/10.1016/j.jvolgeores.2017.02.016

Barreto, C.J.S., Lafon, J.M., De Lima, E.F. and Sommer, C.A. 2016. Geochemical and Sr–Nd–Pb isotopic insight into the low-Ti basalts from southern Paraná Igneous Province, Brazil: the role of crustal contamination. *International Geology Review*, **58**, 1324–1349, https://doi.org/10.1080/00206814.2016.1147988

Bartolini, A. 2003. Cretaceous radiolarian biochronology and carbon isotope stratigraphy of ODP Site 1149 (northwestern Pacific, Nadezhda Basin). *In*: Ludden, J.N., Plank, T. and Escutia, C. (eds) *Proceedings of the Ocean Drilling Program, Scientific Results*, **185**, 1–17, https://doi.org/10.2973/odp.proc.sr.185.011.2003

Bea, F., Montero, P., Haissen, F. and El Archi, A. 2013. 2.46 Ga kalsilite and nepheline syenites from the Awsard pluton, Reguibat Rise of the West African Craton, Morocco. Generation of extremely K-rich magmas at the Archean–Proterozoic transition. *Precambrian Research*, **224**, 242–254, https://doi.org/10.1016/j.precamres.2012.09.024

Belkacim, S., Gasquet, D. *et al.* 2017. The Ediacaran volcanic rocks and associated mafic dykes of the Ouarzazate Group (Anti-Atlas, Morocco): clinopyroxene composition, whole-rock geochemistry and Sr–Nd isotopes constraints from the Ouzellarh–Siroua salient (Tifnoute valley). *Journal of African Earth Sciences*, **127**, 113–135, https://doi.org/10.1016/j.jafrearsci.2016.08.002

Bersezio, R., Erba, E., Gorza, M. and Riva, A. 2002. Berriasian–Aptian black shales of the Maiolica Formation (Lombardian Basin, southern Alps, northern Italy): local to global events. *Palaeogeography, Palaeoclimatology, Palaeoecology*, **180**, 253–275, https://doi.org/10.1016/S0031-0182(01)00416-3

Blanc, A., Bernard-Griffiths, J. *et al.* 1992. U–Pb dating and isotopic signature of the alkaline ring complexes of Bou Naga (Mauritania): its bearing on late Proterozoic plate tectonics around the West African craton. *Journal of African Earth Sciences*, **14**, 301–311, https://doi.org/10.1016/0899-5362(92)90034-A

Boher, M., Abouchami, W., Michard, A., Albarede, F. and Arndt, N.T. 1992. Crustal growth in West Africa at 2.1 Ga. *Journal of Geophysical Research*, **97**, 345–369, https://doi.org/10.1029/91JB01640

Bomou, B., Adatte, T., Tantawy, A.A., Mort, H., Fleitmann, D., Huang, Y. and Föllmi, K.B. 2013. The expression of the Cenomanian–Turonian oceanic anoxic event in Tibet. *Palaeogeography, Palaeoclimatology, Palaeoecology*, **369**, 466–481, https://doi.org/10.1016/j.palaeo.2012.11.011

Bornemann, A. and Mutterlose, J. 2008. Calcareous nannofossil and ^{13}C records from the Early Cretaceous of the western Atlantic Ocean: evidence for enhanced fertilization across the Berriasian–Valanginian transition. *PALAIOS*, **23**, 821–832, https://doi.org/10.2110/palo.2007.p07-076r

Bouloton, J., Gasquet, D. and Pin, C. 2019. Petrogenesis of the Early-Triassic quartz-monzodiorite dykes from Central Jebilet (Moroccan Meseta): trace element and Nd–Sr isotope constraints on magma sources, and inferences on their geodynamic context. *Journal of African Earth Sciences*, **149**, 451–464, https://doi.org/10.1016/j.jafrearsci.2018.08.023

Brassell, S.C. 2009. Steryl ethers in a Valanginian claystone: molecular evidence for cooler waters in the central Pacific during the Early Cretaceous? *Palaeogeography, Palaeoclimatology, Palaeoecology*, **282**, 45–57, https://doi.org/10.1016/j.palaeo.2009.08.009

Carignan, J., Hild, P., Mevelle, G., Morel, J. and Yeghicheyan, D. 2001. Routine analyses of trace elements in geological samples using flow injection and low pressure on-line liquid chromatography coupled to ICP-MS: a study of geochemical reference materials BR, DR-N, UB-N, AN-G and GH. *Geostandards Newsletter*, **25**, 187–198, https://doi.org/10.1111/j.1751-908x.2001.tb00595.x

Carpentier, M., Chauvel, C., Maury, R.C. and Mattielli, N. 2009. The 'zircon effect' as recorded by the chemical and Hf isotopic compositions of Lesser Antilles forearc sediments. *Earth and Planetary Science Letters*, **287**, 86–99, https://doi.org/10.1016/j.epsl.2009.07.043

Carpentier, M., Weis, D. and Chauvel, C. 2013. Large U loss during weathering of upper continental crust: the sedimentary record. *Chemical Geology*, **340**, 91–104, https://doi.org/10.1016/j.chemgeo.2012.12.016

Čepek, P., Gartner, S. and Cool, T. 1980. Mesozoic calcareous nannofossils, Deep Sea Drilling Project sites 415 and 416, Moroccan Basin. *In*: Lancelot, Y. and Winterer, E.L. (eds) *Initial Reports of the Deep Sea Drilling Project*, **50**, 345–351, https://doi.org/10.2973/dsdp.proc.50.108.1980

Chalot-Prat, F. 1995. Genesis of rhyolitic ignimbrites and lavas from distinct sources at a deep crustal level: field, petrographic, chemical and isotopic (Sr, Nd) constraints in the Tazekka volcanic complex (Eastern Morocco). *Lithos*, **36**, 29–49, https://doi.org/10.1016/0024-4937(95)00004-Y

Channell, J.E.T., Erba, E. and Lini, A. 1993. Magnetostratigraphic calibration of the Late Valanginian carbon isotope event in pelagic limestones from northern Italy and Switzerland. *Earth and Planetary Science Letters*, **118**, 145–166, https://doi.org/10.1016/0012-821X(93)90165-6

Charbonnier, G., Boulila, S. *et al.* 2013. Astronomical calibration of the Valanginian 'Weissert' episode: the Orpierre marl–limestone succession (Vocontian Basin, southeastern France). *Cretaceous Research*, **45**, 25–42, https://doi.org/10.1016/j.cretres.2013.07.003

Charbonnier, G., Morales, C., Duchamp-Alphonse, S., Westermann, S., Adatte, T. and Föllmi, K.B. 2017. Mercury enrichment indicates volcanic triggering of Valanginian environmental change. *Scientific Reports*, **7**, 40808, https://doi.org/10.1038/srep40808

Charbonnier, G., Duchamp-Alphonse, S., Deconinck, J.F., Adatte, T., Spangenberg, J.E., Colin, C. and Föllmi, K.B. 2020. A global palaeoclimatic reconstruction for the Valanginian based on clay mineralogical and geochemical data. *Earth-Science Reviews*, **202**, 103092, https://doi.org/10.1016/j.earscirev.2020.103092

Chauvel, C., Lewin, E., Carpentier, M., Arndt, N.T. and Marini, J.C. 2008. Role of recycled oceanic basalt and sediment in generating the Hf–Nd mantle array. *Nature Geoscience*, **1**, 64–67, https://doi.org/10.1038/ngeo.2007.51

Chauvel, C., Bureau, S. and Poggi, C. 2011. Comprehensive chemical and isotopic analyses of basalt and sediment reference materials. *Geostandards and Geoanalytical Research*, **35**, 125–143, https://doi.org/10.1111/j.1751-908X.2010.00086.x

Chauvel, C., Garçon, M., Bureau, S., Besnault, A., Jahn, B.-m. and Ding, Z. 2014. Constraints from loess on the Hf–Nd isotopic composition of the upper continental crust. *Earth and Planetary Science Letters*, **388**, 48–58, https://doi.org/10.1016/j.epsl.2013.11.045

Chavagnac, V., German, C.R. and Taylor, R.N. 2008. Global environmental effects of large volcanic eruptions on ocean chemistry: evidence from 'hydrothermal' sediments (ODP Leg 185, Site 1149B). *Journal of Geophysical Research: Solid Earth*, **113**, https://doi.org/10.1029/2007JB005333

Direen, N.G., Cohen, B.E. *et al.* 2017. Naturaliste Plateau: constraints on the timing and evolution of the Kerguelen large igneous province and its role in Gondwana breakup. *Australian Journal of Earth Sciences*, **64**, 851–869, https://doi.org/10.1080/08120099.2017.1367326

Duchamp-Alphonse, S., Gardin, S., Fiet, N., Bartolini, A., Blamart, D. and Pagel, M. 2007. Fertilization of the northwestern Tethys (Vocontian basin, SE France) during the Valanginian carbon isotope perturbation: evidence from calcareous nannofossils and trace element data. *Palaeogeography, Palaeoclimatology, Palaeoecology*, **243**, 132–151, https://doi.org/10.1016/j.palaeo.2006.07.010

EL Haibi, H., EL Hadi, H. *et al.* 2020. Geochronology and isotopic geochemistry of Ediacaran high-K calc-alkaline felsic volcanism: an example of a Moroccan perigondwanan (Avalonian?) remnant in the El Jadida horst (Mazagonia). *Journal of African Earth Sciences*, **163**, 103669, https://doi.org/10.1016/j.jafrearsci.2019.103669

Ellouz, N., Patriat, M., Gaulier, J.M., Bouatmani, R. and Sabounji, S. 2003. From rifting to Alpine inversion: Mesozoic and Cenozoic subsidence history of some Moroccan basins. *Sedimentary Geology*, **156**, 185–212, https://doi.org/10.1016/S0037-0738(02)00288-9

Erba, E. and Tremolada, F. 2004. Nannofossil carbonate fluxes during the Early Cretaceous: phytoplankton response to nutrification episodes, atmospheric CO_2, and anoxia. *Paleoceanography*, **19**, https://doi.org/10.1029/2003PA000884

Erba, E., Bartolini, A. and Larson, R.L. 2004. Valanginian Weissert oceanic anoxic event. *Geology*, **32**, 149–152, https://doi.org/10.1130/G20008.1

Essaifi, A. and Zayane, R. 2018. Petrogenesis and origin of the Upper Jurassic–Lower Cretaceous magmatism in Central High Atlas (Morocco): major, trace element and isotopic (Sr–Nd) constraints. *Journal of African Earth Sciences*, **137**, 229–245, https://doi.org/10.1016/j.jafrearsci.2017.10.002

Essaifi, A., Samson, S. and Goodenough, K. 2014. Geochemical and Sr–Nd isotopic constraints on the petrogenesis and geodynamic significance of the Jebilet magmatism (Variscan Belt, Morocco). *Geological Magazine*, **151**, 666–691, https://doi.org/10.1017/S0016756813000654

Ewart, A., Schon, R.W. and Chappell, B.W. 1992. The Cretaceous volcanic–plutonic province of the central Queensland (Australia) coast – a rift related 'calc-alkaline' province. *Earth and Environmental Science Transactions of the Royal Society of Edinburgh*, **83**, 327–345, https://doi.org/10.1017/S0263593300008002

Ewart, A., Milner, S.C., Armstrong, R.A. and Duncan, A.R. 1998*a*. Etendeka volcanism of the Goboboseb mountains and Messum Igneous Complex, Namibia. Part I: geochemical evidence of early Cretaceous Tristan plume melts and the role of crustal contamination in the Paraná–Etendeka CFB. *Journal of Petrology*, **39**, 191–225, https://doi.org/10.1093/petroj/39.2.191

Ewart, A., Milner, S.C., Armstrong, R.A. and Duncan, A.R. 1998*b*. Etendeka volcanism of the Goboboseb Mountains and Messum Igneous Complex, Namibia. Part II: Voluminous Quartz Latite Volcanism of the Awahab Magma System. *Journal of Petrology*, **39**, 227–253, https://doi.org/10.1093/petroj/39.2.227

Ewart, A., Marsh, J.S., Milner, S.C., Duncan, A.R., Kamber, B.S. and Armstrong, R.A. 2004*a*. Petrology and geochemistry of Early Cretaceous bimodal continental flood volcanism of the NW Etendeka, Namibia. Part 2: characteristics and petrogenesis of the high-Ti latite and high-Ti and low-Ti voluminous quartz latite eruptives. *Journal of Petrology*, **45**, 107–138, https://doi.org/10.1093/petrology/egg082

Ewart, A., Marsh, J.S., Milner, S.C., Duncan, A.R., Kamber, B.S. and Armstrong, R.A. 2004*b*. Petrology and geochemistry of Early Cretaceous bimodal continental flood volcanism of the NW Etendeka, Namibia. Part 1: introduction, mafic lavas and re-evaluation of mantle source components. *Journal of Petrology*, **45**, 59–105, https://doi.org/10.1093/petrology/egg083

Fesneau, C., Deconinck, J.F., Pellenard, P. and Reboulet, S. 2009. Evidence of aerial volcanic activity during the Valanginian along the northern Tethys margin. *Cretaceous Research*, **30**, 533–539, https://doi.org/10.1016/j.cretres.2008.09.004

Föllmi, K.B. 2012. Early Cretaceous life, climate and anoxia. *Cretaceous Research*, **35**, 230–257, https://doi.org/10.1016/j.cretres.2011.12.005

Föllmi, K.B., Weissert, H., Bisping, M. and Funk, H. 1994. Phosphogenesis, carbon-isotope stratigraphy, and carbonate-platform evolution along the Lower Cretaceous northern Tethyan margin. *GSA Bulletin*, **106**, 729–746, https://doi.org/10.1130/0016-7606(1994)106<0729:PCISAC>2.3.CO;2

Föllmi, K.B., Godet, A., Bodin, S. and Linder, P. 2006. Interactions between environmental change and shallow water carbonate buildup along the northern Tethyan margin and their impact on the Early Cretaceous carbon isotope record. *Paleoceanography and Paleoclimatology*, **21**, https://doi.org/10.1029/2006PA001313

Frey, F.A., McNaughton, N.J., Nelson, D.R., DeLaeter, J.R. and Duncan, R.A. 1996. Petrogenesis of the Bunbury Basalt, Western Australia: interaction between the Kerguelen plume and Gondwana lithosphere? *Earth and Planetary Science Letters*, **144**, 163–183, https://doi.org/10.1016/0012-821x(96)00150-1

Frizon de Lamotte, D., Zizi, M. *et al.* 2008. The Atlas system. *Lecture Notes in Earth Sciences*, **116**, 133–202, https://doi.org/10.1007/978-3-540-77076-3_4

Frizon de Lamotte, D., Leturmy, P. *et al.* 2009. Mesozoic and Cenozoic vertical movements in the Atlas system (Algeria, Morocco, Tunisia): an overview. *Tectonophysics*, **475**, 9–28, https://doi.org/10.1016/j.tecto.2008.10.024

Gale, A.S., Mutterlose, J., Batenburg, S., Gradstein, F.M., Agterberg, F.P., Ogg, J.G. and Petrizzo, M.R. 2020. The Cretaceous Period. *In*: Gradstein, F.M., Ogg, J.G., Schmitz, M.D. and Ogg, G.M. (eds) *Geologic Time Scale 2020*. Elsevier, 1023–1086.

Gasquet, D., Leterrier, J., Mrini, Z. and Vidal, P. 1992. Petrogenesis of the Hercynian Tichka plutonic complex (Western High Atlas, Morocco): trace element and Rb/Sr and Sm/Nd isotopic constraints. *Earth and Planetary Science Letters*, **108**, 29–44, https://doi.org/10.1016/0012-821X(92)90058-4

Gasquet, D., Levresse, G., Cheilletz, A., Azizi-Samir, M.R. and Mouttaqi, A. 2005. Contribution to a geodynamic reconstruction of the Anti-Atlas (Morocco) during Pan-African times with the emphasis on inversion tectonics and metallogenic activity at the Precambrian–Cambrian transition. *Precambrian Research*, **140**, 157–182, https://doi.org/10.1016/j.precamres.2005.06.009

Gréselle, B., Pittet, B. *et al.* 2011. The Valanginian isotope event: a complex suite of palaeoenvironmental perturbations. *Palaeogeography, Palaeoclimatology, Palaeoecology*, **306**, 41–57, https://doi.org/10.1016/j.palaeo.2011.03.027

Gröcke, D.R., Price, G.D., Robinson, S.A., Baraboshkin, E.Y., Mutterlose, J. and Ruffell, A.H. 2005. The Upper Valanginian (Early Cretaceous) positive carbon-isotope event recorded in terrestrial plants. *Earth and Planetary Science Letters*, **240**, 495–509, https://doi.org/10.1016/j.epsl.2005.09.001

Gross, A., Palchan, D., Krom, M.D. and Angert, A. 2016. Elemental and isotopic composition of surface soils from key Saharan dust sources. *Chemical Geology*, **442**, 54–61, https://doi.org/10.1016/j.chemgeo.2016.09.001

Grousset, F.E. and Biscaye, P.E. 2005. Tracing dust sources and transport patterns using Sr, Nd and Pb isotopes. *Chemical Geology*, **222**, 149–167, https://doi.org/10.1016/j.chemgeo.2005.05.006

Grousset, F.E., Rognon, P., Coudé-Gaussen, G. and Pédemay, P. 1992. Origins of peri-Saharan dust deposits traced by their Nd and Sr isotopic composition. *Palaeogeography, Palaeoclimatology, Palaeoecology*, **93**, 203–212, https://doi.org/10.1016/0031-0182(92)90097-O

Grousset, F.E., Parra, M., Bory, A., Martinez, P., Bertrand, P., Shimmield, G. and Ellam, R.M. 1998. Saharan wind regimes traced by the Sr–Nd isotopic composition of subtropical Atlantic sediments: last Glacial Maximum vs today. *Quaternary Science Reviews*, **17**, 395–409, https://doi.org/10.1016/S0277-3791(97)00048-6

Hafid, M., Tari, G. *et al.* 2008. Atlantic basins. *Lecture Notes in Earth Sciences*, **116**, 303–329, https://doi.org/10.1007/978-3-540-77076-3_6

Hawkesworth, C.J., Mantovani, M.S.M., Taylor, P.N. and Palacz, Z. 1986. Evidence from the Prana of south Brazil for a continental contribution to the Dupal basalts. *Nature*, **322**, 356–359, https://doi.org/10.1038/322356a0

Hennig, S., Weissert, H. and Bulot, L. 1999. C-isotope stratigraphy, a calibration tool between ammonite- and magnetostratigraphy: the Valanginian–Hauterivian transition. *Geologica Carpathica*, **50**, 91–96.

Jaffey, A.H., Flynn, K.F., Glendenin, L.E., Bentley, W.C. and Essling, A.M. 1971. Precision measurement of half-lives and specific activities of ^{235}U and ^{238}U. *Physical Review C*, **4**, 1889–1906, https://doi.org/10.1103/PhysRevC.4.1889

Jenkyns, H.C. 2003. Evidence for rapid climate change in the Mesozoic–Palaeogene greenhouse world. *Philosophical Transactions of the Royal Society A: Mathematical, Physical and Engineering Sciences*, **361**, 1885–1916, https://doi.org/10.1098/rsta.2003.1240

Jenkyns, H.C. 2010. Geochemistry of oceanic anoxic events. *Geochemistry, Geophysics, Geosystems*, **11**, https://doi.org/10.1029/2009GC002788

Jochum, K.P., Wilson, S.A. *et al.* 2011. GSD-1G and MPI-DING reference glasses for in situ and bulk isotopic determination. *Geostandards and Geoanalytical Research*, **35**, 193–226, https://doi.org/10.1111/j.1751-908X.2010.00114.x

Jud, R. 1994. *Biochronology and systematics of Early Cretaceous Radiolaria of the western Tethys*. PhD thesis, Université de Lausanne.

Kuhn, O., Weissert, H., Föllmi, K.B. and Hennig, S. 2005. Altered carbon cycling and trace-metal enrichment during the late Valanginian and early Hauterivian. *Eclogae Geologicae Helvetiae*, **98**, 333–344, https://doi.org/10.1007/s00015-005-1172-7

Kujau, A., Heimhofer, U., Ostertag-Henning, C., Gréselle, B. and Mutterlose, J. 2012. No evidence for anoxia during the Valanginian carbon isotope event – an organic–geochemical study from the Vocontian Basin, SE France. *Global and Planetary Change*, **92–93**, 92–104, https://doi.org/10.1016/j.gloplacha.2012.04.007

Kujau, A., Heimhofer, U. *et al.* 2013. Reconstructing Valanginian (Early Cretaceous) mid-latitude vegetation and climate dynamics based on spore–pollen assemblages. *Review of Palaeobotany and Palynology*, **197**, 50–69, https://doi.org/10.1016/j.revpalbo.2013.05.003

Kumar, A., Abouchami, W., Galer, S.J.G., Garrison, V.H., Williams, E. and Andreae, M.O. 2014. A radiogenic isotope tracer study of transatlantic dust transport from Africa to the Caribbean. *Atmospheric Environment*, **82**, 130–143, https://doi.org/10.1016/j.atmosenv.2013.10.021

Kump, L.R. and Arthur, M.A. 1999. Interpreting carbon-isotope excursions: carbonates and organic matter. *Chemical Geology*, **161**, 181–198, https://doi.org/10.1016/S0009-2541(99)00086-8

Küster, D., Liégeois, J.P., Matukov, D., Sergeev, S. and Lucassen, F. 2008. Zircon geochronology and Sr, Nd, Pb isotope geochemistry of granitoids from Bayuda Desert and Sabaloka (Sudan): evidence for a Bayudian event (920–900 Ma) preceding the Pan-African orogenic cycle (860–590 Ma) at the eastern boundary of the Saharan Metacra. *Precambrian Research*, **164**, 16–39, https://doi.org/10.1016/j.precamres.2008.03.003

Lancelot, Y., Winterer, E.L. *et al.* 1980. Site 416, in the Moroccan Basin, Deep Sea Drilling Project Leg 50. *Initial Reports of the Deep Sea Drilling Project*, **50**, 115–301, https://doi.org/10.2973/dsdp.proc.50.104.1980

Le Roex, A.P. and Lanyon, R. 1998. Isotope and trace element geochemistry of Cretaceous Damaraland lamprophyres and carbonatites, northwestern Namibia: evidence for plume–lithosphere interactions. *Journal of Petrology*, **39**, 1117–1146, https://doi.org/10.1093/petroj/39.6.1117

Le Roux, L.J. and Glendenin, L.E. 1963. Half-life of ^{232}Th. *In*: *Proceedings of the National Meeting on Nuclear Energy*, Pretoria, South Africa, April 1963, 83–94.

Lini, A., Weissert, H. and Erba, E. 1992. The Valanginian carbon isotope event: a first episode of greenhouse climate conditions during the Cretaceous. *Terra Nova*, **4**, 374–384, https://doi.org/10.1111/j.1365-3121.1992.tb00826.x

Liu, Z., Zhou, Q., Lai, Y., Qing, C., Li, Y., Wu, J. and Xia, X. 2015. Petrogenesis of the Early Cretaceous Laguila bimodal intrusive rocks from the Tethyan Himalaya: implications for the break-up of Eastern Gondwana. *Lithos*, **236–237**, 190–202, https://doi.org/10.1016/j.lithos.2015.09.006

Lozar, F. and Tremolada, F. 2003. Calcareous nannofossil biostratigraphy of Cretaceous sediments recovered at ODP Site 1149 (Leg 185, Nadezhda Basin, western Pacific). *In*: Ludden, J.N., Plank, T. and Escutia, C. (eds) *Proceedings of the Ocean Drilling Program, Scientific Results*, **185**, 1–21, https://doi.org/10.2973/odp.proc.sr.185.010.2003

Marques, L.S., Dupré, B. and Piccirillo, E.M. 1999. Mantle source compositions of the Paraná magmatic province (southern Brazil): evidence from trace element and Sr–Nd–Pb isotope geochemistry. *Journal of Geodynamics*, **28**, 439–458, https://doi.org/10.1016/S0264-3707(99)00020-4

Marques, L.S., De Min, A., Rocha-Júnior, E.R.V., Babinski, M., Bellieni, G. and Figueiredo, A.M.G. 2018. Elemental and Sr–Nd–Pb isotope geochemistry of the Florianópolis dyke swarm (Paraná magmatic province): crustal contamination and mantle source constraints. *Journal of Volcanology and Geothermal Research*, **355**, 149–164, https://doi.org/10.1016/j.jvolgeores.2017.07.005

Martinez, M., Deconinck, J.F., Pellenard, P., Riquier, L., Company, M., Reboulet, S. and Moiroud, M. 2015. Astrochronology of the Valanginian–Hauterivian stages (Early Cretaceous): chronological relationships between the Paraná–Etendeka large igneous province and the Weissert and the Faraoni events. *Global and Planetary Change*, **131**, 158–173, https://doi.org/10.1016/j.gloplacha.2015.06.001

Mattioli, E., Pittet, B., Riquier, L. and Grossi, V. 2014. The mid-Valanginian Weissert Event as recorded by calcareous nannoplankton in the Vocontian Basin. *Palaeogeography, Palaeoclimatology, Palaeoecology*, **414**, 472–485, https://doi.org/10.1016/j.palaeo.2014.09.030

McArthur, J.M., Janssen, N.M.M., Reboulet, S., Leng, M.J., Thirlwall, M.F. and van de Schootbrugge, B. 2007. Palaeotemperatures, polar ice-volume, and isotope stratigraphy (Mg/Ca, $\delta^{18}O$, $\delta^{13}C$, $^{87}Sr/^{86}Sr$): the Early Cretaceous (Berriasian, Valanginian, Hauterivian). *Palaeogeography, Palaeoclimatology, Palaeoecology*, **248**, 391–430, https://doi.org/10.1016/j.palaeo.2006.12.015

Meyer, I., Davies, G.R. and Stuut, J.B.W. 2011. Grain size control on Sr–Nd isotope provenance studies and impact on paleoclimate reconstructions: an example from deep-sea sediments offshore NW Africa. *Geochemistry, Geophysics, Geosystems*, **12**, https://doi.org/10.1029/2010GC003355

Mingram, B., Trumbull, R.B., Littman, S. and Gerstenberger, H. 2000. A petrogenetic study of anorogenic felsic magmatism in the Cretaceous Paresis ring complex, Namibia: evidence for mixing of crust and mantle-derived components. *Lithos*, **54**, 1–22, https://doi.org/10.1016/S0024-4937(00)00033-5

Montero, P., Haissen, F., El Archi, A., Rjimati, E. and Bea, F. 2014. Timing of Archean crust formation and cratonization in the Awsard–Tichla zone of the NW Reguibat Rise, West African Craton: a SHRIMP, Nd–Sr isotopes, and geochemical reconnaissance study. *Precambrian Research*, **242**, 112–137, https://doi.org/10.1016/j.precamres.2013.12.013

Morales, C., Kujau, A. *et al.* 2015. Palaeoclimate and palaeoenvironmental changes through the onset of the Valanginian carbon-isotope excursion: evidence from the Polish Basin. *Palaeogeography, Palaeoclimatology, Palaeoecology*, **426**, 183–198, https://doi.org/10.1016/j.palaeo.2015.03.013

O'Nions, R.K., Carter, S.R., Evensen, N.M. and Hamilton, P.J. 1979. Geochemical and cosmochemical applications of Nd isotope analysis. *Annual Review of Earth and Planetary Sciences*, **7**, 11–38, https://doi.org/10.1146/annurev.ea.07.050179.000303

Ouajhain, B., Daoudi, L., Medina, F. and Rocha, F. 2009. Contrôle paléogéographique de la sédimentation argileuse du Jurassique du bassin atlasique d'Essaouira (haut atlas occidental, Maroc). *Comunicações Geológicas*, **96**, 51–66.

Patchett, P.J., White, W.M., Feldmann, H., Kielinczuk, S. and Hofmann, A.W. 1984. Hafnium/rare earth element fractionation in the sedimentary system and crustal recycling into the Earth's mantle. *Earth and Planetary Science Letters*, **69**, 365–378, https://doi.org/10.1016/0012-821X(84)90195-X

Pawlig, S., Gueye, M., Klischies, R., Schwarz, S., Wemmer, K. and Siegesmund, S. 2006. Geochemical and Sr–Nd isotopic data on the Birimian of the Kedougou–Kenieba Inlier (Eastern Senegal): implications on the Palaeoproterozoic evolution of the West African Craton. *South African Journal of Geology*, **109**, 411–427, https://doi.org/10.2113/gssajg.109.3.411

Peate, D.W. 2009. Global dispersal of Pb by large-volume silicic eruptions in the Paraná–Etendeka large igneous province. *Geology*, **37**, 1071–1074, https://doi.org/10.1130/G30338A.1

Peate, D.W. and Hawkesworth, C.J. 1996. Lithospheric to asthenospheric transition in low-Ti flood basalts from southern Paraná, Brazil. *Chemical Geology*, **127**, 1–24, https://doi.org/10.1016/0009-2541(95)00086-0

Peate, D.W., Hawkesworth, C.J., Mantovani, M.M.S., Rogers, N.W. and Turner, S.P. 1999. Petrogenesis and stratigraphy of the high-Ti/Y Urubici magma type in the Paraná flood basalt province and implications for the nature of 'Dupal'-type mantle in the South Atlantic region. *Journal of Petrology*, **40**, 451–473, https://doi.org/10.1093/petroj/40.3.451

Peucat, J.J., Capdevila, R., Drareni, A., Choukroune, P., Fanning, C.M., Bernard-Griffiths, J. and Fourcade, S. 1996. Major and trace element geochemistry and isotope (Sr, Nd, Pb, O) systematics of an Archaean basement involved in a 2.0 Ga very high-temperature (1000°C) metamorphic event: in Ouzzal Massif, Hoggar, Algeria. *Journal of Metamorphic Geology*, **14**, 667–692, https://doi.org/10.1111/j.1525-1314.1996.00054.x

Peucat, J.J., Capdevila, R., Drareni, A., Mahdjoub, Y. and Kahoui, M. 2005. The Eglab massif in the West African Craton (Algeria), an original segment of the Eburnean orogenic belt: petrology, geochemistry and geochronology. *Precambrian Research*, **136**, 309–352, https://doi.org/10.1016/j.precamres.2004.12.002

Piqué, A., Le Roy, P. and Amrhar, M. 1998. Transtensive synsedimentary tectonics associated with ocean opening: the Essaouira–Agadir segment of the Moroccan Atlantic margin. *Journal of the Geological Society, London*, **155**, 913–928, https://doi.org/10.1144/gsjgs.155.6.0913

Plank, T. and Ludden, J.N. 1992. Geochemistry of sediments in the Argo Abyssal Plain at Site 765: a continental margin reference section for sediment recycling in subduction zones. *In*: Ludden, J.N.,Gradstein, F.M. *et al.* (eds) *Proceedings of the Ocean Drilling Program, Scientific Results*, **123**, 167–189, https://doi.org/10.2973/odp.proc.sr.123.158.1992

Plank, T., Ludden, J.N. *et al.* 2000. Site 1149. *Proceedings of the Ocean Drilling Program, Initial Results*, **185**, 1–190, https://doi.org/10.2973/odp.proc.ir.185.104.2000

Plank, T., Kelley, K.A., Murray, R.W. and Stern, L.Q. 2007. Chemical composition of sediments subducting at the Izu–Bonin trench. *Geochemistry, Geophysics, Geosystems*, **8**, 1–16, https://doi.org/10.1029/2006GC001444

Poulsen, C.J., Seidov, D., Barron, E.J. and Peterson, W.H. 1998. The impact of paleogeographic evolution on the surface oceanic circulation and the marine environment within the Mid-Cretaceous Tethys. *Paleoceanography*, **13**, 546–559, https://doi.org/10.1029/98PA01789

Price, G.D. and Mutterlose, J. 2004. Isotopic signals from late Jurassic–early Cretaceous (Volgian–Valanginian) sub-Arctic belemnites, Yatria River, Western Siberia. *Journal of the Geological Society, London*, **161**, 959–968, https://doi.org/10.1144/0016-764903-169

Price, G.D., Sellwood, B.W. and Valdes, P.J. 1995. Sedimentological evaluation of general circulation model simulations for the 'greenhouse' Earth: Cretaceous and Jurassic case studies. *Sedimentary Geology*, **100**, 159–180, https://doi.org/10.1016/0037-0738(95)00106-9

Price, G.D., Janssen, N.M.M., Martinez, M., Company, M., Vandevelde, J.H. and Grimes, S.T. 2018. A high-resolution belemnite geochemical analysis of early Cretaceous (Valanginian–Hauterivian) environmental and climatic perturbations. *Geochemistry, Geophysics, Geosystems*, **19**, 3832–3843, https://doi.org/10.1029/2018GC007676

Rämö, O.T., Heikkilä, P.A. and Pulkkinen, A.H. 2016. Geochemistry of Paraná–Etendeka basalts from Misiones, Argentina: some new insights into the petrogenesis of high-Ti continental flood basalts. *Journal of South American Earth Sciences*, **67**, 25–39, https://doi.org/10.1016/j.jsames.2016.01.008

Reboulet, S., Mattioli, E., Pittet, B., Baudin, F., Olivero, D. and Proux, O. 2003. Ammonoid and nannoplankton abundance in Valanginian (early Cretaceous) limestone–marl successions from the southeast France Basin: carbonate dilution or productivity? *Palaeogeography, Palaeoclimatology, Palaeoecology*, **201**, 113–139, https://doi.org/10.1016/S0031-0182(03)00541-8

Reboulet, S., Jaillard, E., Shmeit, M., Giraud, F., Masrour, M. and Spangenberg, J.E. 2022. Biostratigraphy, carbon isotope and sequence stratigraphy of South Tethyan Valanginian successions in the Essaouira–Agadir Basin (Morocco). *Cretaceous Research*, **140**, 105341, https://doi.org/10.1016/j.cretres.2022.105341

Rocha, B.C., Janasi, V.A. *et al.* 2020. Rapid eruption of silicic magmas from the Paraná magmatic province (Brazil) did not trigger the Valanginian event. *Geology*, **48**, 1174–1178, https://doi.org/10.1130/G47766.1

Rocha-Júnior, E.R.V., Marques, L.S., Babinski, M., Nardy, A.J.R., Figueiredo, A.M.G. and Machado, F.B. 2013. Sr–Nd–Pb isotopic constraints on the nature of the mantle sources involved in the genesis of the high-Ti tholeiites from northern Paraná continental flood basalts (Brazil). *Journal of South American Earth Sciences*, **46**, 9–25, https://doi.org/10.1016/j.jsames.2013.04.004

Rudnick, R.L. and Gao, S. 2013. Composition of the continental crust. *In*: Rudnick, R.L. (ed.) *Treatise on Geochemistry (Second Edition). Vol. 4: The Crust*. Elsevier, 1–51, https://doi.org/10.1016/B978-0-08-095975-7.00301-6

Sauzéat, L., Rudnick, R.L., Chauvel, C., Garçon, M. and Tang, M. 2015. New perspectives on the Li isotopic composition of the upper continental crust and its weathering signature. *Earth and Planetary Science Letters*, **428**, 181–192, https://doi.org/10.1016/j.epsl.2015.07.032

Schlanger, S.O. and Jenkyns, H.C. 1976. Cretaceous oceanic anoxic events: causes and consequences *Geologie en Mijnbouw*, **55**, 179–184.

Scholle, P.A. and Arthur, M.A. 1980. Carbon isotope fluctuations in Cretaceous pelagic limestones: potential stratigraphic and petroleum exploration tool. *AAPG Bulletin*, **64**, 67–87, https://doi.org/10.1306/2F91892D-16CE-11D7-8645000102C1865D

Scotese, C.R. 2016. *PALEOMAP PaleoAtlas for GPlates and the PaleoData Plotter Program, PALEOMAP Project*, http://www.scotese.com

Shmeit, M., Giraud, F., Jaillard, E., Reboulet, S., Masrour, M., Spangenberg, J.E. and El-Samrani, A. 2022. The Valanginian Weissert Event on the south Tethyan margin: a dynamic paleoceanographic evolution based on the study of calcareous nannofossils. *Marine Micropaleontology*, **175**, 102134, https://doi.org/10.1016/j.marmicro.2022.102134

Skonieczny, C., Bory, A. *et al.* 2013. A three-year time series of mineral dust deposits on the West African margin: sedimentological and geochemical signatures and implications for interpretation of marine paleo-dust records. *Earth and Planetary Science Letters*, **364**, 145–156, https://doi.org/10.1016/j.epsl.2012.12.039

Sprovieri, M., Coccioni, R., Lirer, F., Pelosi, N. and Lozar, F. 2006. Orbital tuning of a lower Cretaceous composite record (Maiolica Formation, central Italy). *Paleoceanography and Paleoclimatology*, **21**, PA4212, https://doi.org/10.1029/2005PA001224

Tapsoba, B., Lo, C.H., Jahn, B.M., Chung, S.L., Wenmenga, U. and Iizuka, Y. 2013. Chemical and Sr–Nd isotopic compositions and zircon U–Pb ages of the Birimian granitoids from NE Burkina Faso, West African Craton: implications on the geodynamic setting and crustal evolution. *Precambrian Research*, **224**, 364–396, https://doi.org/10.1016/j.precamres.2012.09.013

Thirlwall, M.F. 1991. Long-term reproducibility of multicollector Sr and Nd isotope ratio analysis. *Chemical Geology*, **94**, 85–104, https://doi.org/10.1016/S0009-2541(10)80021-X

Thompson, R.N., Gibson, S.A., Dickin, A.P. and Smith, P.M. 2001. Early Cretaceous basalt and picrite dykes of the Southern Etendeka Region, NW Namibia: windows into the role of the Tristan mantle plume in Paraná–Etendeka magmatism. *Journal of Petrology*, **42**, 2049–2081, https://doi.org/10.1093/petrology/42.11.2049

Toummite, A., Liegeois, J.P., Gasquet, D., Bruguier, O., Beraaouz, E.H. and Ikenne, M. 2013. Field, geochemistry and Sr–Nd isotopes of the Pan-African granitoids from the Tifnoute Valley (Sirwa, Anti-Atlas, Morocco): a post-collisional event in a metacratonic setting. *Mineralogy and Petrology*, **107**, 739–763, https://doi.org/10.1007/s00710-012-0245-3

Trumbull, R.B., Harris, C., Frindt, S. and Wigand, M. 2004. Oxygen and neodymium isotope evidence for source diversity in Cretaceous anorogenic granites from Namibia and implications for A-type granite genesis. *Lithos*, **73**, 21–40, https://doi.org/10.1016/j.lithos.2003.10.006

Turner, S.P., Kirstein, L.A., Hawkesworth, C.J., Peate, D.W., Hallinan, S. and Mantovani, M.S.M. 1999. Petrogenesis of an 800 m lava sequence in eastern Uruguay: insights into magma chamber processes beneath the Paraná flood basalt province. *Journal of Geodynamics*, **28**, 471–487, https://doi.org/10.1016/S0264-3707(99)00022-8

Van De Schootbrugge, B., Kuhn, O., Adatte, T., Steinmann, P. and Föllmi, K. 2003. Decoupling of P- and C_{org}-burial following Early Cretaceous (Valanginian–Hauterivian) platform drowning along the NW Tethyan margin. *Palaeogeography, Palaeoclimatology, Palaeoecology*, **199**, 315–331, https://doi.org/10.1016/S0031-0182(03)00540-6

Villa, I.M., De Bièvre, P., Holden, N.E. and Renne, P.R. 2015. IUPAC-IUGS recommendation on the half life of ^{87}Rb. *Geochimica et Cosmochimica Acta*, **164**, 382–385, https://doi.org/10.1016/j.gca.2015.05.025

Villa, I.M., Holden, N.E., Possolo, A., Ickert, R.B., Hibbert, D.B. and Renne, P.R. 2020. IUPAC-IUGS recommendation on the half-lives of ^{147}Sm and ^{146}Sm. *Geochimica et Cosmochimica Acta*, **285**, 70–77, https://doi.org/10.1016/j.gca.2020.06.022

Weissert, H. 1989. C-Isotope stratigraphy, a monitor of paleoenvironmental change: a case study from the early Cretaceous. *Surveys in Geophysics*, **10**, 1–61, https://doi.org/10.1007/BF01901664

Weissert, H., Lini, A., Föllmi, K.B. and Kuhn, O. 1998. Correlation of Early Cretaceous carbon isotope stratigraphy and platform drowning events: a possible link? *Palaeogeography, Palaeoclimatology, Palaeoecology*, **137**, 189–203, https://doi.org/10.1016/S0031-0182(97)00109-0

Westermann, S., Föllmi, K.B. *et al.* 2010. The Valanginian δ^{13}C excursion may not be an expression of a global oceanic anoxic event. *Earth and Planetary Science Letters*, **290**, 118–131, https://doi.org/10.1016/j.epsl.2009.12.011

Westermann, S., Duchamp-Alphonse, S., Fiet, N., Fleitmann, D., Matera, V., Adatte, T. and Föllmi, K.B. 2013. Paleoenvironmental changes during the Valanginian: new insights from variations in phosphorus contents and bulk- and clay mineralogies in the western Tethys. *Palaeogeography, Palaeoclimatology, Palaeoecology*, **392**, 196–208, https://doi.org/10.1016/j.palaeo.2013.09.017

White, W.M., Albarède, F. and Télouk, P. 2000. High-precision analysis of Pb isotope ratios by multi-collector ICP-MS. *Chemical Geology*, **167**, 257–270, https://doi.org/10.1016/S0009-2541(99)00182-5

Wortmann, U.G. and Weissert, H. 2000. Tying platform drowning to perturbations of the global carbon cycle with a delta $\delta^{13}C_{Org}$-curve from the Valanginian of DSDP Site 416. *Terra Nova*, **12**, 289–294, https://doi.org/10.1046/j.1365-3121.2000.00312.x

Zhu, D., Mo, X. *et al.* 2008. Petrogenesis of the earliest Early Cretaceous mafic rocks from the Cona area of the eastern Tethyan Himalaya in south Tibet: interaction between the incubating Kerguelen plume and the eastern Greater India lithosphere? *Lithos*, **100**, 147–173, https://doi.org/10.1016/j.lithos.2007.06.024

Zhu, D., Chung, S.L., Mo, X.X., Zhao, Z.D., Niu, Y., Song, B. and Yang, Y.H. 2009. The 132 Ma Comei-Bunbury large igneous province: remnants identified in present-day southeastern Tibet and southwestern Australia. *Geology*, **37**, 583–586, https://doi.org/10.1130/G30001A.1